Published in 2012. Geoderma. 185-186: 84-96.

Constraining soil mineral weathering $^{87}Sr/^{86}Sr$ for calcium apportionment studies of a deciduous forest growing on soils developed from granitoid igneous rocks

Nicolas Bélanger[1], Chris Holmden[2], Francois Courchesne[3], Benoît Côté[4] and William H. Hendershot[4]

[1]Centre d'étude de la forêt, UER Sciences et technologies, Teluq, Université du Québec, Montréal, Québec, Canada, H2X 3P2 (e-mail: belanger.nicolas@teluq.ca);

[2]Saskatchewan Isotope Laboratory, Department of Geological Sciences, University of Saskatchewan, Saskatoon, Saskatchewan, Canada, S7N 5E2;

[3]Département de Géographie, Université de Montréal, Montréal, QC, Canada, H3C 3J7;

[4]Department of Natural Resource Sciences, McGill University, Macdonald Campus, Ste-Anne-de-Bellevue, QC, Canada, H9X 3V9.

Abstracts: We used $^{87}Sr/^{86}Sr$ as a proxy for Ca to apportion the contribution of atmospheric deposition and soil mineral weathering sources to the Ca pools in trees in a small forested watershed of southern Quebec. The effects of topography and forest stand composition were assessed by dividing the watershed into three study zones representing two elevations and differences in tree species. Apportionment calculations show that all tree species studied contained Ca that is dominantly sourced from soil mineral weathering (averaging 85%), due to the presence in the soils of easily weathered Ca-bearing minerals such as calcite and apatite as well as the relatively deep rooting habits (reaching the mineral soil) of the tree species. Calcium pools in trees are shifted towards the atmospheric component on hilltops due to the filtering of dry aerosols of the tree canopies which are more exposed to atmospheric circulation than trees at the bottom of the slopes, although some variability in soil bulk chemistry and mineralogy in the watershed obscures the full extent of this phenomenon. The buildup and recycling of Ca in the soil-vegetation system, with the forest floor acting as the major accessible Ca pool for the tree roots, must be considered when interpreting apportionment calculations. This work supports other Ca cycling models in forests suggesting that topography can influence the balance of Ca captured from atmospheric sources by trees, even in cases where mineral weathering is the dominant source of Ca nutrition in trees.

Keywords: Deciduous forest, sugar maple, calcium cycling, atmospheric deposition, soil mineral weathering, strontium isotopes, $^{87}Sr/^{86}Sr$, calcium to strontium ratios, Ca/Sr, barium to strontium ratios, Ba/Sr, forest floor, tree calcium pools.

Introduction

Calcium (Ca) is an important nutrient for tree growth and can influence stand productivity in temperate and boreal forests, notably in sugar maple (*Acer saccharum*) stands (Kobe et al., 1995; van Breemen et al., 1997). However, several factors such as soil acidification (Likens et al., 1996), intensive silviculture and fast tree growth (Alban, 1982) and forest harvesting (Thiffault et al., 2006) have the potential to lower Ca availability and in turn, alter tree nutrition, health and growth rates. It follows that certain measures to protect the forest floor may be necessary in ecosystems that efficiently retain and reuse recycled Ca within the first few centimeters of soil (Dijkstra and Smits, 2002; Holmden and Bélanger, 2010). Calcium cycling and tree nutrition must therefore be well understood in boreal and temperate forests in view of optimizing the management of soil and forest resources.

Over the last twenty years, biogeochemists and soil scientists have used the isotopes of strontium (Sr) as a proxy for Ca to apportion the contribution of atmospheric deposition and soil mineral weathering to the Ca pools in trees [e.g. see Table 1 in Bélanger and Holmden (2010)]. In components of terrestrial environments, the amount of ^{87}Sr varies as a result of the slow radioactive decay of ^{87}Rb. The $^{87}Sr/^{86}Sr$ ratio can therefore be used as a tracer of Sr sources in natural systems. If $^{87}Sr/^{86}Sr$ in atmospheric deposition differs from that of soil mineral weathering, then these sources will be mixed in trees through uptake of Sr by fine roots and released again to the soil through litterfall and throughfall. As the geochemical behaviour of Sr is close to that of Ca, the Ca/Sr and $^{87}Sr/^{86}Sr$ ratios of atmospheric deposition and soil mineral weathering as well as the mixed $^{87}Sr/^{86}Sr$ ratios in the trees can be used in a mass balance to determine the fractions

of Ca contributed by the two primary sources. For this method to work, the field site must meet three conditions to ensure the reliability of the $^{87}Sr/^{86}Sr$ technique: (1) the $^{87}Sr/^{86}Sr$ signatures of the weathering and atmospheric end-members are sufficiently contrasting, (2) the variability in the end-member $^{87}Sr/^{86}Sr$ signatures must be small, and (3) the mixing of Sr and Ca in the soil-plant system must be conservative. For a review of applications demonstrating the potential of $^{87}Sr/^{86}Sr$ as a tracer in soils and forested ecosystems, see Stewart et al. (1998) and Capo et al. (1998).

The $^{87}Sr/^{86}Sr$ studies of Ca apportioning in trees and soils have changed our understanding of the sources of base cations in terrestrial ecosystems. Before the use of this approach, it was believed that soil mineral weathering was the main (or sole) contributor of Ca to trees. It is now recognized that the atmosphere, either from wet or dry deposition, is an important source of Ca in many settings. In fact, some forests seem to satisfy their Ca requirements almost entirely from atmospheric inputs (Kennedy et al., 1998; Drouet et al., 2005; Perakis et al., 2006; Poszwa et al., 2009; Bélanger and Holmden, 2010), whereas, in others, Ca nutrition is mostly supported by soil mineral weathering (Bailey et al., 1996; Vitousek et al., 1999; Blum et al., 2002; Bern et al., 2005). Some other forests depend on a mixture of these two primary Ca sources (Miller et al., 1993; Blum et al., 2002; Poszwa et al., 2004; Bélanger and Holmden, 2010). These studies suggest that it varies mainly as a function of the atmospheric Ca flux, the weathering susceptibility of Ca-containing minerals (e.g. apatite), and the topographic position and rooting habits (depth) of the tree species.

Application of the $^{87}Sr/^{86}Sr$ tracer technique to forests growing on soils developed from granitoid igneous rocks is complicated by the fact that the $^{87}Sr/^{86}Sr$ of soil mineral

weathering is difficult to assess and that uncertainties may be large. This is because the minerals weather at widely varying rates and may have highly contrasting $^{87}Sr/^{86}Sr$ ratios. Determining the mineral weathering contribution through laboratory leaching experiments is a common approach but it has potential pitfalls. Indeed, many choices must be made that can affect the outcome of the results (Bailey et al., 1996; Drouet et al., 2005, 2007; Holmden and Bélanger, 2010). For example, should a sample of the unweathered rock material be prepared for acid leaching, or should a sample from the existing soil profile be used? If the natural soil is chosen, then at what depth should it be collected? Natural soil horizons do not weather evenly and new minerals form over time. Furthermore, ion exchange sites deep in the soil profile may contain recycled Sr that has percolated down from upper horizons (Holmden and Bélanger, 2010). The type of acid, the acid strength and the temperature of the acid treatment and whether the soils are sieved or ground to test for a specific particle size or bulk composition have also been shown to affect the $^{87}Sr/^{86}Sr$ ratio of the laboratory inferred weathering signature. Although much progress has been made towards developing a set of best laboratory practices for determining the mineral weathering signature of soil and rock samples (Blum et al., 2002; Bullen and Bailey, 2005; Nezat et al., 2007; Bélanger and Holmden, 2010; Holmden and Bélanger, 2010), improving our ability to predict the $^{87}Sr/^{86}Sr$ of soil mineral weathering in polymineralic soils remains a challenge and is crucial for Ca apportioning studies in boreal and temperate forests because many of these forest are supported by such soils.

The focus of this study is a sugar maple forest of southern Quebec, Canada, growing on soils developed from granitoid igneous rocks and characterized by a complex

mixture of minerals. $^{87}Sr/^{86}Sr$ ratios of trees, soil solutions, atmospheric deposition, streamwater and soil leachates are measured and combined with Ca/Sr in a mass balance to determine the fractions of Ca contributed by atmospheric deposition and soil mineral weathering.

Materials & Methods

Study site

The study was conducted in the Hermine experimental watershed (HEW) at the *Station de Biologie des Laurentides* (SBL) *de l'Université de Montréal*, Quebec, in the Lower Laurentians, 80 km north of Montreal. Thirty-year average precipitation at SBL is 1100 mm, with 30% falling as snow. Mean annual temperature is 3.6°C. The forest has a mean basal area of 28 m^2 ha^{-1} and is dominated by sugar maple (*Acer saccharum*), red maple (*Acer rubrum*) and American beech (*Fagus grandifolia*). The top of the hillslopes was disturbed by fire in the 1920s which also resulted in patches of early successional tree species such as largetooth aspen (*Populus grandidentata*), yellow birch (*Betula alleghaniensis*) and paper birch (*Betula papyrifera*) (Bélanger et al., 2002a).

The soils are well-drained rocky glacial tills derived partly from the underlying anorthosite pluton of the Morin Anorthosite Complex (Philpotts, 1966; Doig, 1991). However, due to the small size of the pluton, the soils in the watershed have also acquired a mineral composition that originates from a variety of more felsic rocks (charnockite, mangerite, jotunite and syenite) located in the periphery of the anorthosite complex (Figure 1) which were mixed with the anorthosite by continental ice sheets during the Pleistocene. As a result, the major element composition of the bulk soils is relatively

homogenous across the watershed but differs markedly from the underlying anorthositic bedrock (Table 1).

The mineralogy of the <2 µm (clay) fraction of the podzolic B horizons was estimated by McCourt (1993) using X-ray diffraction on Mg-, K- and HCl-treated samples. The procedures of Kittrick and Hope (1963) were used to separate the clays into semi-quantitative percentages of the whole <2 µm fraction. These estimates suggest 45.4% quartz, 15% plagioclase feldspars, 19% chlorite, 10% muscovite, 4% hornblende, 4% vermiculite, 1.5% biotite, 1% garnet and 0.1% apatite. Elemental analysis results were also used to assign elements to their respective minerals using the UPPSALA norms for soils (Sverdrup and Warfvinge, 1992). The UPPSALA model is a normative back-calculation model for reconstructing empirical soil mineralogy from total digestion analysis and is based on assumptions of the stoichiometric composition of the minerals in soils of granitic origin (i.e., Swedish Precambrian Shield). Minerals are grouped into assemblies of minerals with similar composition and dissolution rates (e.g. chlorite is composed of trioctahedral chlorite, primary illite, trioctahedral vermiculite of primary type, and biotite; epidote includes all epidotes and pyroxenes). These norms suggest 34.1% quartz, 29% plagioclase feldspars, 15.7% hornblende, 13.8% K-feldspars, 4.9% muscovite, 2.1% epidote and 0.4% apatite. Plagioclase makes up between 15 wt.% of the clays (X-ray diffraction) and 29 wt.% of the bulk soil (UPPSALA norms), which is a proxy of the maximum contribution of anorthosite to the whole soil considering it is nearly a monomineralic rock composed of plagioclase feldspars (~90% based on CIPW norms using the major element composition of the anorthosite in Table 1).

The soils have a sandy loam texture and are classified as Orthic Humo-Ferric Podzols (Soil Classification Working Group, 1998). The forest floor is a moder humus form varying in depth from 5 to 10 cm. The significant presence of vermiculite and chlorite in the local soils as suggested by X-ray diffraction indicates that the alteration of biotite (K-saturated) to vermiculite (Mg-saturated) is a common weathering reaction in cool and wet soils (Blum and Erel, 1997; Wilson, 2004), whereas chlorite is most likely present due to hydrothermal alteration of biotite as the igneous rocks cooled or during post-magmatic hydrothermal activity (Hurlbut and Klein, 1985).

Field study

This study is part of an ongoing long-term monitoring program initiated in 1993 at HEW aimed at examining the effects of intra- and inter-year climatic variations and of long-term changes in atmospheric deposition on nutrient availability and cycling as well as forest health (Côté et al., 1998; Côté et al., 2003; Bélanger et al., 2002b, 2004; Courchesne et al., 2005).

Three zones that reflect the spatial variability of tree species, soils and topography in the watershed were selected. Zone 1 (downstream-downslope) and zone 2 (upstream-downslope) are dominated by sugar maple, whereas zone 3 (downstream-upslope) is mainly composed of largetooth aspen and birch spp. Zone 3 is similar in elevation to zone 2 but different topographically because it is on a plateau that may affect the drainage. Within each zone, three circular plots of 300 m^2 were delineated for detailed studies. We used soils sampled during the summer of 1993 to avoid disturbing the plots with a large pedon as hydrochemical studies linking streamwater chemistry with soil solutions and

shallow groundwater are ongoing. They were sampled by diagnostic horizons (LFH, Ae, Bf_1, Bf_2, BC and parent C) up to about 1 m in one pedon within each plot.

Zero-tension lysimeters (Hendershot and Courchesne, 1991) were installed below the forest floor and rooting zone (50 cm) at the same time of soil sampling in 1993. A tower reaching above the forest canopy (ca. 25 m) was constructed in 1993 to sample bulk deposition. This sampler was installed just outside the watershed in the uppermost section of a hillslope. Funnel collectors of 17.5 cm in diameter are connected to high density polyethylene bottles using Tygon ® tubing. All equipment is carefully acid-washed with 10% HNO_3 solutions before use. A white plastic cup is installed on top of the bottle to prevent direct exposure to sunlight and thus evaporation. The tower was damaged after a major windstorm in 2000 and a new one had to be built at a different location. Since 1993, soil solutions and bulk deposition have been sampled monthly from November to April and bi-monthly from May to October. For this study, we made up bulk samples using a series of soil solution and bulk deposition samples collected during specific periods of 2004 (Table 2). We also compared our 2004 bulk deposition results with another five bulk deposition samples and five wet-only deposition samples collected in May and June of 2009. The wet-only samples were collected from an automated and chemically clean wet-only deposition collector (Ecotech Model 200, Blackburn, Australia) placed on a raft in the center of a small lake (lac Triton) near the bulk deposition tower or from the provincial wet-only deposition monitoring station (Boulet and Jacques, 1992). Both wet-only samplers were within 500 m of the tower.

Stream discharge was calculated in 2004 from the water level above a 908 V-notch weir measured with a Global Level sensor bubbler (model BT101). The

measurement frequency was four per hour (Biron et al., 1999). Daily stream water samples collected in 2004 at the weir using an automated water sampler just downstream of zone 1 were also used for this study. Stream water samples were bulked (volume weighted) according to seasonality to account for any change in isotopic or elemental composition following a change in hydrological conditions (Table 2). The stream water chemical and isotopic signatures at low flow at HEW can possibly be used as a proxy for anorthosite weathering based on the premise that the stream, under such hydrological conditions, is almost entirely fed by shallow groundwater in direct contact with the bedrock (O'Brien and Hendershot, 1993). This premise will be validated in the course of evaluating soil mineral weathering at HEW using $^{87}Sr/^{86}Sr$ ratios and major and minor element chemistry.

Foliage in the upper tier of the canopy was sampled randomly from three to six trees of various tree species within each plot (n = 39) in the third week of August of 2004. Stem wood of the various tree species was sampled randomly (n = 16) in mid-May of 2006 with a 4.1 mm-diameter Haglöf® increment borer in plots of zones 1 and 3 only. Foliage and stem wood samples were oven-dried for 48 h at 65ºC and then finely ground (about 50 μm). Foliage and the outer 10 cm of the stem wood, excluding the bark, were digested in a clean room environment at 80°C for 16 hours. Both PTFE beakers and ultra pure HNO_3 were used for the procedure.

Sequential chemical leaching

Due to the chemical and mineralogical differences of the soils relative to the local anorthosite bedrock, the soil mineral weathering signature for $^{87}Sr/^{86}Sr$ and molar Ca/Sr

ratios was derived from weak acid treatments of soils and the anorthosite collected from the study site, rather than by analysis of the anorthosite alone. A sequential chemical leach of the lower B horizon was performed on one sample per zone following a protocol very similar to that used by Blum et al. (2002) and Nezat et al. (2007). The lower B horizon was selected as it relates to the depth at which the mineral soil solutions (50 cm) were collected by lysimetry. Thus, the chemical composition of lower B solutions and soil leachates should, in theory, be comparable. Using Ca/Sr, potassium (K)/sodium (Na), Ca/P, and other elemental ratios for the leachates, this approach was used successfully to constrain $^{87}Sr/^{86}Sr$ of a soil mineral (e.g. apatite) or a series of soil minerals (e.g. K-bearing phyllosilicates or plagioclase) (Blum et al., 2002; Nezat et al., 2007; 2008; Bélanger and Holmden, 2010). A 3 g sample was first placed in contact with 30 ml of 1 M NH_4Cl solution for 2 h on an end-over-end shaker to remove exchangeable Ca and Sr. The sample was then leached for 2 h on the same shaker with 30 ml of 1 M HNO_3 at room temperature (20-21°C). The third step was to further leach the 1 M HNO_3 leached soils in 50 mL centrifuge tubes with 15 M HNO_3 for 10 h at 80˚C. Finally, aliquots of the residues of those three successive reactions were transferred to individual PTFE beakers and completely dissolved with a mixture of concentrated HF and HNO_3 acids for 48 h at 120°C. All of the leachates were evaporated to dryness and re-dissolved in 0.2 N HNO_3 for major and minor element analysis. The same stock solutions were used for $^{87}Sr/^{86}Sr$ analysis. Nezat et al. (2007, 2008) suggested that the 1 M HNO_3 leach attacks calcite and apatite in direct contact with the solution, although phyllosilicates, hornblende and epidote can be dissolved to some extent (Bélanger and Holmden, 2010). The 15 M HNO_3 leach attacks phyllosilicates, hornblende and other more resistant minerals such as K-

feldspars. The concentrated HF-HNO_3 leach dissolves the remaining mineral residues as well as the K-feldspars, plagioclase and quartz.

In another sequential procedure, the same soil samples were reacted with a 1 M NH_4Cl solution and then leached with a 30 ml 0.1 M HCl solution for 2 h. The 0.1 M HCl leach was initially proposed by Miller et al. (1993) as a reasonable treatment to simulate the release of Sr from anorthosite weathering for the purpose of determining its $^{87}Sr/^{86}Sr$ signature, whereas Drouet et al. (2005) suggested that the 0.1 M HCl leach mostly dissolves calcite.

Lastly, a finely ground sample (~50 μm) of the local anorthosite was subjected to the following series of leachates: (1) 1 M NH_4Cl only, (2) 0.1 M HCl only, (3) 1 M HNO_3 only, (4) 1 M NH_4Cl followed by 0.1 M HCl, and (5) 1 M NH_4Cl followed by 0.1 M HCl and 1 M HNO_3.

Major and minor element analyses

Bulk solution samples identified in Table 2 and the ten 2009 bulk and wet-only deposition samples were all analyzed for Ca, phosphorus (P), K, magnesium (Mg), rubidium (Rb), Sr, Ba and $^{87}Sr/^{86}Sr$ absorption spectrophotometry after filtration of the samples through 0.45 μm polycarbonate membranes. Total dissolved elemental analysis was performed on a Perkin Elmer Elan6000 quadrupole ICP-MS. Instrument operating conditions are detailed in Simonetti et al. (2008). External reproducibility, based on repeated analysis of international whole rock standards (e.g. BCR-1, BE-N), is 5-10% (2 σ level) of the quoted abundances for most elements.

The elemental compositions of the solid phase of the lower B horizons and of anorthosite presented in Table 1 were determined on 32-mm-diameter fused beads prepared from a 1:5 soil-lithium tetraborate mixture using an automated X-ray fluorescence spectrometer system (Philips PW2440 4 kW) with a Rhodium 60 kV end window X-ray tube. A thin section of the anorthosite was also prepared for the *in situ* measurement of the major elements in selected minerals using a JEOL 8600 Superprobe in the Earth and Atmospheric Sciences Department at the University of Alberta.

$^{87}Sr/^{86}Sr$ analyses

Sample preparation and $^{87}Sr/^{86}Sr$ analysis were performed in the Radiogenic Isotope Facility at the University of Alberta. Strontium was separated from matrix cations using conventional cation exchange chromatography prior to mass spectrometry following techniques described in Sharp et al. (2002). Strontium isotopic analyses of atmospheric deposition samples (bulk and wet-only) were performed by Thermal Ionization Mass Spectrometry on a Thermo Fisher Triton instrument using a static data collection mode and tantalum (Ta) filaments with a phosphoric acid and Ta gel mixture to increase ionization efficiency (Creaser et al., 2004). All $^{87}Sr/^{86}Sr$ analyses were corrected for instrumental mass fractionation using an exponential law and $^{86}Sr/^{88}Sr=0.1194$. A ratio of 0.710245 was obtained for the NIST SRM 987 Sr isotopic standard. For all other samples, Sr isotopic compositions were measured using a NuPlasma MC-ICP-MS instrument following techniques described in Buzon et al. (2007) and Simonetti et al. (2008). Accuracy and reproducibility of $^{87}Sr/^{86}Sr$ analyses were verified by repeated

analyses of a 100 ppb solution of NIST SRM 987, which yielded an average value of 0.710242 ± 0.000041 (2σ standard deviation; n=13 analyses).

Results

Atmospheric deposition $^{87}Sr/^{86}Sr$ and molar Ca/Sr

Atmospheric deposition $^{87}Sr/^{86}Sr$ ratios range between 0.7087 and 0.7133. The 2004 and 2009 medians are respectively 0.7120 and 0.7095 (Table 2). We could not detect any difference in $^{87}Sr/^{86}Sr$ (P=0.265) and molar Ca/Sr (P=0.403) ratios between the three types of samplers based on one-way ANOVA (SigmaPlot 12, Systat Software Inc., Illinois). The average $^{87}Sr/^{86}Sr$ ratio in precipitation (all samples) over the two years is 0.7104 ±0.0015 (1σ), whereas the average molar Ca/Sr ratio is 555 ±180. These results are consistent with $^{87}Sr/^{86}Sr$ ratios reported by Simonetti et al. (2000) for southern Quebec snow and reflect variation in the contributions of continental and marine sources of Sr.

Wood and foliage $^{87}Sr/^{86}Sr$ and molar Ca/Sr

Wood and foliage $^{87}Sr/^{86}Sr$ ratios are higher at the top (zones 2 and 3) of the hill than at the bottom (Table 3). All species show the same relationship between topography and $^{87}Sr/^{86}Sr$ ratios of wood and foliage. The average value for foliage is 0.7077 ±0.0001 (1σ) in zone 1, 0.7085 ±0.0003 in zone 2 and 0.7082 ±0.0001 in zone 3. These values are significantly different at $p < 0.001$ according to a Holm-Sidak test after a one-way ANOVA. A similar topographical pattern is also observed in wood and foliage molar Ca/Sr ratios but that is mostly due to our samples changing from mostly sugar maple in

zone 1 and 2 to a mixture of birch spp., maple spp., American beech and aspen in zone 3, which reflects the species composition of the forest at HEW. Red maple, birch spp. and American beech always has higher leaf molar Ca/Sr ratios compared to sugar maple and aspen.

Soil and bedrock $^{87}Sr/^{86}Sr$, molar Ca/Sr and molar Ba/Sr

Soil acid leachates and digests of the residues of the lower B horizon from each of the three zones show a strong linear trend on a $^{87}Sr/^{86}Sr$ vs. molar Ca/Sr diagram (Figure 2), which reflects differences in mineral weathering susceptibility. Using the weak 0.1 M HCl leach, the easily weathered mineral component in the soil is defined as having low $^{87}Sr/^{86}Sr$ (~0.7070) and high molar Ca/Sr (~1625) ratios. This signature is consistent with the weathering of low K, high Ca bearing trace minerals such as calcite and apatite.

The more resistant mineral component (i.e., 1 M HNO_3 treatment) has high $^{87}Sr/^{86}Sr$ (0.7089-0.7131) and low Ca/Sr (524-1365), reflecting Sr released from K-bearing minerals such as biotite and other phyllosilicates, which are also low in Ca. The stronger soil acid leachates (i.e., concentrated HNO_3 and HF-HNO_3) yield the highest $^{87}Sr/^{86}Sr$ ratios (≥0.7124-0.7157) and lowest molar Ca/Sr ratios (97-383). The residues reflect the weathering of resistant minerals such as K-feldspar and plagioclase.

The $^{87}Sr/^{86}Sr$ ratios of the anorthosite powders are also negatively correlated with molar Ca/Sr ratios, but the slope is small and the relationship is weaker (r^2=0.50) due mainly to the much smaller range in $^{87}Sr/^{86}Sr$ ratios (0.7066-0.7078) compared to the soil acid leachates (Figure 2). The relationship is driven by a molar Ca/Sr ratio of 814 which was obtained with the 0.1 M HCl leach after extraction using 1 M NH_4Cl. This high

molar Ca/Sr ratio likely reflects contributions from trace calcite, which is a minor constituent of the anorthosite.

A plot of $^{87}Sr/^{86}Sr$ vs. P shows that apatite is contributing Sr and Ca to the leachates of the soils (Figure 3). Based on the observed covariant trend, more P is released in the 0.1 M HCl leach than in the subsequently applied weak and strong HNO_3 leachates, which is consistent with the high solubility of igneous apatite. Although the anorthosite contains apatite, no P was released by the 0.1 M HCl or stronger 1.0 N HNO_3 treatment. The CIPW norms suggest very small amounts of apatite (0.04%) in the anorthosite. The soil and anorthosite leach results thus suggest that apatite in anorthosite is armoured by other minerals that resist 0.1 M HCl or 1.0 N HNO_3 and that the traces of apatite in anorthosite are not the main source of apatite in the till soils.

A plot of $^{87}Sr/^{86}Sr$ vs. molar Mg/Sr shows that large amounts of Mg are released in the 15 M HNO_3 treatment compared to the other treatments (Figure 4). This is consistent with increased dissolution of biotite and chlorite in the presence of stronger acids.

Stream water and soil solution $^{87}Sr/^{86}Sr$, molar Ca/Sr and molar Ba/Sr

Stream water molar Ca/Sr and Ba/Sr ratios collected at both high and low flows over the 2004 hydrological year show strong covariant trends with $^{87}Sr/^{86}Sr$ ratios, indicative of mixing between two components (Figure 5). The component with high $^{87}Sr/^{86}Sr$ has low molar Ca/Sr (Figure 5a) and high molar Ba/Sr (Figure 5b), whereas the component with low $^{87}Sr/^{86}Sr$ is the opposite. The range in molar Ca/Sr is quite limited (~6%) in comparison to molar Ba/Sr which range by about an order of magnitude (from

0.3 to 1.8). The correlations between stream discharge and stream water $^{87}Sr/^{86}Sr$, molar Ca/Sr and Ba/Sr as well as Sr concentrations are relatively strong (Figure 6) and also indicate changes in the mixing of hydrological components during the year. There are some inconsistencies in the $^{87}Sr/^{86}Sr$ and molar Ba/Sr relationship with the months of August and October, which both show relatively high stream $^{87}Sr/^{86}Sr$ (0.7077-0.7078) and molar Ba/Sr (0.98-1.29) despite its low flow.

The linearity in the stream water trends for $^{87}Sr/^{86}Sr$ vs. molar Ca/Sr and Ba/Sr is indicative of two component mixing. One component is anorthosite, which has a molar Ba/Sr ratio of 0.18±0.03, based on the weak acid treatments applied to the powdered sample. On the $^{87}Sr/^{86}Sr$ vs. molar Ba/Sr diagram, the stream trend intersects the anorthosite leachate trend at the $^{87}Sr/^{86}Sr$ ratio of 0.7074 (Figure 5b). The intersection is well determined owing to the very uniform molar Ba/Sr ratios of the anorthosite leachates. It appears that the stream chemistry at low flow is dominated by weathering of anorthosite, which crops out in the stream. By contrast, the elevated $^{87}Sr/^{86}Sr$ ratio of the stream at high flow is due to Sr and Ca inputs from soil solutions, which feed the stream during large rainfall events. The supporting evidence is the median $^{87}Sr/^{86}Sr$ and molar Ca/Sr ratios of the forest floor and mineral soil solutions, which plot on an extension of the stream water trend line towards higher $^{87}Sr/^{86}Sr$ ratios (Figure 7a,b).

Calcium apportionment calculations

The Ca in trees (*veg*) is apportioned between soil mineral weathering (*w*) and atmospheric deposition (*a*) derived Ca inputs using the following equation:

$$\frac{Ca_a}{Ca_{veg}} = \frac{Ca_a}{Ca_a + Ca_w} = \frac{\left(\frac{Sr}{Ca}\right)_w \left[\left(\frac{^{87}Sr}{^{86}Sr}\right)_w - \left(\frac{^{87}Sr}{^{86}Sr}\right)_{veg}\right]}{\left(\frac{Sr}{Ca}\right)_a \left[\left(\frac{^{87}Sr}{^{86}Sr}\right)_{veg} - \left(\frac{^{87}Sr}{^{86}Sr}\right)_a\right] + \left(\frac{Sr}{Ca}\right)_w \left[\left(\frac{^{87}Sr}{^{86}Sr}\right)_w - \left(\frac{^{87}Sr}{^{86}Sr}\right)_{veg}\right]}$$

A derivation of this equation can be found in Stewart et al. (1998). Because the $^{87}Sr/^{86}Sr$ ratios in trees changes between the bottom (0.7077) and top of the hill (0.7081 and 0.7085), the apportionment calculations are performed separately for each of the three zones. The atmospheric deposition end-member used is the $^{87}Sr/^{86}Sr$ (0.7104) and molar Ca/Sr (555) of precipitation at the study site averaged over the 2004 and 2009 seasons (Table 2). Using these data for the calculations, results in Table 4 show that soil mineral weathering is the dominant source of Ca to the trees at HEW, accounting for 85% of the contributions when averaged over all three zones. When the data are examined spatially, there is doubling of atmospherically derived Ca inputs between the bottom and top of the hill. Uncertainties with these apportionment calculations are small considering that results vary by less than 5% when replacing the average $^{87}Sr/^{86}Sr$ and molar Ca/Sr ratios of atmospheric deposition in the mixing equation with the upper or lower values of the (1 sigma) standard deviation (Table 2).

The correctness of the Ca apportionment results rather rests on the validity of the inferred end-members to mixing. It is possible, for example, that the Ca contribution from atmospheric deposition is even lower than calculated above owing to the fact that its high $^{87}Sr/^{86}Sr$ ratio overlaps with the $^{87}Sr/^{86}Sr$ ratio of Sr released from the soils by the more aggressive acid soil leachates (i.e. phyllosilicate weathering). It is therefore possible that the intermediate range $^{87}Sr/^{86}Sr$ ratios in the trees is due to mixing between two groupings of minerals in the soils: (1) calcite and apatite with low $^{87}Sr/^{86}Sr$ ratios (as before), and

(2) phyllosilicates with high $^{87}Sr/^{86}Sr$ ratios (0.7111) calculated from the average of the 1.0 M HNO_3 leachates (following NH_4Cl and 0.1 M HCl). The apportioning results are virtually the same as above (Table 4), only that the Ca formerly derived from atmospheric deposition in scenario no. 1 (i.e. average atmospheric deposition) is now attributed to the weathering of a phyllosilicate component in the soils with a similar $^{87}Sr/^{86}Sr$ ratio.

Discussion

Soil mineral weathering

In spite of the fact that bedrock lithology at HEW is anorthosite (a rock composed predominantly of plagioclase), the soils have developed almost wholly from the thin veneer of glacial till, which contains a more complicated assemblage of minerals. The study site is situated approximately five kilometers west of a contact zone with anorthosite-orthopyroxene granitoids and southeast of a series of banded granitic gneisses, charnockite gneiss, orthopyroxene granitoids (charnockite, mangerite, jotunite and syenite) and sparse areas of marble (Figure 1). Glacial advance from the north (Veillette, 2004) resulted in a mixing of minerals and rock fragments sampled from the surrounding felsic rocks containing minerals such as quartz, muscovite, plagioclase, K-feldspar, hornblende and biotite, and marbles containing calcite (Peck et al., 2005). Only small amounts of anorthosite (e.g., plagioclase and pyroxene) could have been mixed with other rock types based on the abundance of plagioclase in the soils (29 wt.% of bulk soil).

The meaning behind the range in $^{87}Sr/^{86}Sr$ ratios in the soil acid leachates can be comprehended by plotting the $^{87}Sr/^{86}Sr$ ratios of the soil and anorthosite acid leachates (i.e. HCl, HNO_3 and HNO_3-HF) against the $^{87}Rb/^{86}Sr$ ratios, which are the coordinates of an isochron diagram used for dating rocks and minerals (Figure 8). Comparing the leachate data with the isochron constructed from a nearby mangerite pluton provides another perspective on the nature of the protolith rocks that were mixed by the glacier to form the local till. Such an approach was similarly used in other studies (e.g. Blum and Erel, 1997; Bullen and Bailey 2005). The mangerite isochron age is 1030 ±41Ma and the 'initial' $^{87}Sr/^{86}Sr$ ratio is 0.705 (y-intercept) (Barton and Doig, 1977). This age is similar to the U-Pb zircon age of the Morin Anorthosite dated at 1155 ± 3 Ma (Doig, 1991). The initial $^{87}Sr/^{86}Sr$ ratio has special significance. It is the inferred ratio of the mangerite magma at the time of emplacement. Magmatic minerals with low Rb contents, such as calcite, apatite and plagioclase, will record this signature at the present day. By contrast, $^{87}Sr/^{86}Sr$ ratios of K-bearing minerals such as biotite and K-feldspar will increase over geological time due to additions of ^{87}Sr caused by ^{87}Rb decay.

The soil and anorthosite leachate data in Figure 8 define a linear array with a slope that is very close to the mangerite isochron, albeit with a greater scatter. This is evidence that the chemical and mineralogical makeup of the till soil is similar to the mangerite and that the soil protolith is broadly similar in age to the mangerite rocks (due to the similarity in slope between the soil pseudo-isochron and the mangerite isochron). The minerals of which the soil is composed range from Rb poor to Rb rich, which is again similar to the minerals in the mangerite. The initial $^{87}Sr/^{86}Sr$ ratio for the till derived pseudo-isochron (0.7070) is higher than the mangerite, which is explained by the

documented heterogeneity in the $^{87}Sr/^{86}Sr$ ratios of the magmas from which the rocks of the Morin Anorthosite Complex were formed, owing to crustal contamination of the parent magmas during emplacement (Barton and Doig, 1977).

Knowing the susceptibilities of minerals to dissolution by acids of differing type and strength, several conclusions may be drawn from the pseudo-isochron regarding the soils at HEW. First, the bulk soils are mostly derived from the surrounding orthopyroxene bearing granitoid rocks mixed during Pleistocene ice sheet advances. The local anorthosite bedrock is either a minor component of the bulk soils or is not present at all. Second, the range of $^{87}Sr/^{86}Sr$ ratios in the soil leachates reflects Sr release from two groupings of minerals consistent with the mineralogy of the orthopyroxene granitoids. The first grouping contains abundant Rb (and K) and therefore yields a high $^{87}Sr/^{86}Sr$ ratio. Among the minerals detected by X-ray diffraction in the clay fraction of the soils, biotite and muscovite have such signatures. The high Mg levels and $^{87}Sr/^{86}Sr$ ratios associated with the 15 M HNO_3 soil leachates (Figure 4), which aggressively attacks phyllosilicates (Nezat et al., 2007; Bélanger and Holmden, 2010), points to the possibility that some of the biotite has been altered to chlorite (19%) and vermiculite (4%).

The second grouping has virtually no Rb and a low $^{87}Sr/^{86}Sr$ ratio, indicative of minerals such as plagioclase feldspar and hornblende, but the high molar Ca/Sr ratios of these leachates points to calcite or apatite as the main source of Ca in this grouping. Apatite is a likely candidate based on the strong negative correlation between $^{87}Sr/^{86}Sr$ and P (or correlations with molar Ca/P and Sr/P ratios, Figure 3) in the weak acid leachates (Blum et al., 2002). Calcite is also a likely candidate as indicated by the fact that the 0.1 M HCl leach produced the lowest $^{87}Sr/^{86}Sr$ and highest molar Ca/Sr of all the

soil leachates (Figure 2) (Drouet et al., 2005). The high molar Ca/Sr of 1625 is typical of calcite with small amounts of Sr substitution, but it is also typical of apatite minerals. For example, in geochemical study of world rivers, Gaillardet et al. (1999) reported an average Ca/Sr ratio of ~1400 for rivers draining bedrock composed dominantly of old marine carbonates. Similarly, Holmden et al. (1997) identified an end-member Ca/Sr ratio of 2000 (Sr/Ca = 0.5 millimole/mole) using literature data on world rivers taken from a variety of sources, which they too attributed to the weathering of calcite in watersheds dominated by carbonate bedrock. But because the stoichiometry of apatite is fixed at a molar Ca/P ratio of 1.66, it is possible to calculate the proportion of apatite and calcite contributing the Ca based on the molar Ca/P ratios of that 0.1 M HCl leach (Figure 3d). This soil mineral group in zone 1 is estimated at 41% apatite and 59% calcite, whereas this group is estimated at 12% apatite and 88% calcite in zone 2 and 57% apatite and 43% calcite in zone 3.

The calcite in the soils may be derived from several bedrock sources outcropping in the region, including Phanerozoic marine carbonates, Proterozoic marbles and original igneous calcite from calc-silicate skarn assemblages in rocks of the Morin series (Peck et al., 2005) gathered and mixed into the till by Pleistocene ice sheets moving towards the South (Figure 1). At HEW, F. Courchesne (personal communication) has also measured high Ca concentrations (mean of 5.61 mg l^{-1} with a maximum value of 9.30 mg l^{-1}) in shallow wells (80 cm from surface) collecting groundwater from clay-rich pond sediments. This is about two-fold the mean and peak concentration values of soil solutions collected at 50 cm. The solution pH also varies between 6.6 and 7.6, a level that has never been measured before in any hydrological end-members of the watershed.

Furthermore, the mineralogical analysis (X-ray diffraction) of these pond sediments substantially differs from soil mineralogy. These surprising results suggest a contribution from calcareous material to the surficial geology of the site which is not clearly signalled by X-ray diffraction data or other analyses of the parent till material. Interestingly, the $^{87}Sr/^{86}Sr$ and Ca/Sr ratios of the two 1 M HNO_3 treatments (i.e. with and without an HCl step prior to HNO_3) diverged substantially, with the treatment including the HCl step producing higher $^{87}Sr/^{86}Sr$ and lower molar Ca/Sr ratios (Figure 2). These provide further evidence that less available calcite surfaces were available for the 1 M HNO_3 treatment after leaching with 0.1 M HCl. Similarly, the local anorthosite was leached with an array of acids and our results indicate that the 0.1 M HCl leach after a 1 M NH_4Cl extraction of the rock powders produced the lowest $^{87}Sr/^{86}Sr$ and highest molar Ca/Sr ratios and had a P concentration below the detection limit (P results not shown), suggesting once more the dissolution of calcite. The potential role of calcite as a source of Ca in well-drained acidic forest soils of the Precambrian Shield is often neglected but appears to be important at HEW considering the geology of the surrounding area.

Significance of anorthosite weathering contributions to the stream

Stream water molar Ba/Sr and Ca/Sr ratios are well correlated with $^{87}Sr/^{86}Sr$ ratios (Figures 5 and 7), while $^{87}Sr/^{86}Sr$, molar Ba/Sr and molar Ca/Sr ratios are well correlated with stream discharge (Figure 6). The extrapolation of the stream water data regression line on the $^{87}Sr/^{86}Sr$ vs. molar Ca/Sr plot (Figure 7a) crosses the points depicted by the forest floor and mineral soil solution data (high $^{87}Sr/^{86}Sr$) and the anorthosite acid leachates (low $^{87}Sr/^{86}Sr$). At low flow during the summer (and all of the winter), the

stream exhibited low $^{87}Sr/^{86}Sr$, low molar Ba/Sr and higher molar Ca/Sr, indicative of direct contributions from groundwater in contact with the anorthosite pluton. Conversely, at high flow during spring melt (and the wet month of September), the stream exhibited high $^{87}Sr/^{86}Sr$, high molar Ba/Sr and lower molar Ca/Sr, indicative of contributions from soil solutions.

It therefore appears that the $^{87}Sr/^{86}Sr$ ratios of stream water during the low flow winter months is contributed from the weathering of the local anorthosite, either from the fractured bedrock or large rock fragments deep in the parent material, which is dominated by plagioclase feldspar. This is consistent with the hydrograph separation conducted by O'Brien and Hendershot (1993) at HEW suggesting that groundwater controls the chemical composition of stream water at low flow. In another study, Ali et al. (2010) used end-member mixing analysis (EMMA model) at HEW to identify the main hydrological components contributing to the stream during 64 hydrological events and showed that both the forest floor and shallow mineral soil solutions were becoming significant sources of water to the stream during events with antecedent moisture conditions. They pointed to both the upstream-downslope and downstream-downslope locations (i.e. zones 2 and 1, respectively) as being the main sources of shallow soil solutions to the stream. In our study, the stream water $^{87}Sr/^{86}Sr$, molar Ca/Sr and molar Sr/Ba ratios at high flow fall closer to the forest floor and mineral soil solutions data in zone 1 than the two other zones (see Figure 7b for $^{87}Sr/^{86}Sr$ vs. molar Ba/Sr ratios), supporting the role of this downstream-downslope location in feeding the stream during wet periods. Furthermore, Ali et al. (2008) showed that the mineral soil solutions of upstream-downslope (zone 2) and downstream-upslope (zone 3) locations were more

directly connected to the stream than forest floor solutions from these locations, which is also consistent with Figure 7a,b.

Although weathering of anorthosite bedrock dominates the chemistry of the stream at low flow, it is not an important source of base cations to plant available soil pools and trees of the watershed. Yet, the trends in chemistry and $^{87}Sr/^{86}Sr$ ratios of first order streams have been used in a few Ca apportionment studies to deduce the $^{87}Sr/^{86}Sr$ ratio of the soil mineral weathering end-member (e.g., Kennedy et al., 2002). The idea is that the $^{87}Sr/^{86}Sr$ ratio of a stream at low flow is shifted to the soil mineral weathering end-member, whereas it is shifted to the atmospheric end-member at high flow. In our study, we find that the stream shifts towards soil solution chemistry at high flow but is still dominated by bedrock weathering. Because soils are not formed from the local bedrock, the weathering of the soil cannot be deduced from the weathering of the bedrock at this location. Also, the $^{87}Sr/^{86}Sr$ signature of precipitation may be masked at high flow by shallow groundwater inputs from saturated soils along the stream bank and hillslope. This is a problem that will affect formerly glaciated landscapes. It could also be a problem in soils developed directly from the local bedrock (e.g., laterites) where the weathering interface is very deep and the $^{87}Sr/^{86}Sr$ signature of weathering deep in the profile is decoupled from vegetation while still governing the chemistry of streamwater (Pett-Ridge et al., 2009a).

Implications for Ca apportionment studies using $^{87}Sr/^{86}Sr$ as a tracer

The proportion of atmospherically Ca inputs to the trees in zone 1 (downstream-downslope) is among the lower values found in the literature (see Table 1 in Bélanger

and Holmden (2010)). Recently, forests in Costa Rica (Bern et al. 2005) and Puerto Rico (Pett-Ridge et al. 2009b) growing on deeply weathered mountain soils were unexpectedly shown to be dominated by soil mineral weathering sources of Sr and geological processes. In zone 1 at HEW, the wetter soils close to the stream, due to wetting of reactive mineral surfaces, were modeled (using SAFE) to weather at a greater rate than the soils in the drier downstream-upslope zone 3 (Bélanger et al., 2002b). The simulated release of Ca from soil mineral weathering was indeed about 20% higher than that of the higher elevation plots in zone 3 (Table 4). Trees in that downstream-downslope zone may therefore rely more heavily on soil mineral weathering because of faster weathering. As suggested by Kennedy et al. (2002), species and rooting depth could be important factors in determining the contributions of atmospheric deposition to the Sr and Ca pool in trees. The rooting habit of American beech, largetooth aspen, red maple and white birch is presumably shallower than the associated yellow birch and sugar maple (Burns and Honkala, 1990). The deeper rooting habits of sugar maple and yellow birch, which are the species that constitute most of our foliage database, could therefore potentially mean that soil mineral weathering of calcite and apatite is a more reliable source of Sr and Ca to these tree species. However, neither beech, aspen, red maple or white birch showed $^{87}Sr/^{86}Sr$ differences with sugar maple and yellow birch. This is probably because the former species have tap roots that can easily penetrate the soil to 1 m and/or their rooting patterns do not differ enough from those of yellow birch and sugar maple for Ca and Sr sources in the soil to change substantially.

The higher proportions of atmospherically derived Ca in hilltop trees at HEW also suggests that these canopies are better suited to filtering atmospheric aerosols as they are

more exposed to atmospheric circulation compared to shielded canopies in the valley bottoms (Parker, 1983). The input of high soluble particles from captured aerosols are transferred as throughfall and stemflow to the forest floor (and eventually tree roots). This is seen with the $^{87}Sr/^{86}Sr$ ratios of the forest floor solutions which appear to acquire a Sr isotopic composition that falls close to that of atmospheric deposition (Figure 7, Table 2). The similarity between $^{87}Sr/^{86}Sr$ ratios of mineral soil solutions and atmospheric deposition is not as high because the $^{87}Sr/^{86}Sr$ ratios of mineral soil solutions are largely influenced by mineral weathering. Bélanger and Holmden (2010) also reported hillslope changes in the proportion of atmospherically derived Ca in trees in a mixedwood watershed of northern Saskatchewan, Canada. Using $^{87}Sr/^{86}Sr$ as a tracer of Ca sources, it was determined that trees growing at the bottom of the hillslope received between 40% and 60% of their Ca from atmospheric sources, while those at the uppermost sections of watershed received as much as 90%. Similarly, in a volcanic watershed of Japan, Nakano et al. (2001) showed that trees growing near the stream received ~40% of their Ca from atmospheric sources, while those at higher elevation received 80%. In this case, however, the potential for increased filtering of atmospheric aerosols by trees at higher elevations was not considered. Rather, the results were attributed to changes in the chemical and mineralogical characteristics of the soil along the toposequence.

The soils at HEW are more uniform than those at the northern Saskatchewan or Japanese sites. The similar weathering $^{87}Sr/^{86}Sr$ signature along the hillslope at HEW removes some of the complexity exhibited at the other two sites where different soil mineral weathering $^{87}Sr/^{86}Sr$ ratios had to be considered for each topographic position. The original finding in northern Saskatchewan that elevation is a key factor in the

capturing of atmospheric aerosols is therefore reinforced by the present Quebec study. Yet, the difference in apportionment calculations between zones 1 and 2 (12%) is about 2-fold the difference between zones 1 and 3 (5%), which supports the idea that the canopy filtering effect works in combination with other factors to differentiate Ca sources to the trees between valley bottoms and hilltops. Despite that the soils are drier on hilltops and weather slower (Bélanger et al., 2002b), there is a possibility that the difference in atmospherically derived Ca in the trees between the zones at HEW could be due to landscape differences in soil weathering contributions of Ca from phyllosilicate minerals. An examination of the bulk chemistry data from the soils (Table 1) provides some evidence for a larger felsic component (lower Ca and higher Al) in the upstream-downslope positions (zone 2) compared to zones 1 and 3. The 0.1 M HCl soil leachates in zone 2 also diverged slightly from zones 1 and 3, with zone 2 presenting a higher $^{87}Sr/^{86}Sr$ ratio and a lower molar Ca/Sr ratio. This supports the results in scenario 2 showing a role of the soil phyllosilicate mineral group in providing Ca to the trees. The higher $^{87}Sr/^{86}Sr$ ratios in trees in zone 2 are therefore not only due to increased filtering of atmospheric aerosols but to a change in the type of minerals present in the soil. The increased proportion of atmospherically derived Ca in the trees with elevation due to increased filtering of dry particulates is therefore likely more in the range of 5% (difference between zones 1 and 3) than 12% (difference between zones 1 and 2).

An alternative interpretation of the hillslope influence over Ca apportioning at HEW could be that mineral soils on hilltops have acidified at a faster rate compared to mineral soils near the stream due to higher acidic deposition (Joslin et al., 1992). According to Bullen and Bailey (2005), more atmospherically derived Sr and Ca in

hilltop trees could be explained by the fact that the rooting system of the trees progressively became shallower and is now mainly located in the forest floor where solutions are more largely influenced by Ca originating from the atmosphere. However, Courchesne et al. (2005) did not observe clear evidence for accelerated soil acidification of hilltop soils at HEW. We therefore believe that the filtering of dry particulates by trees on hilltops is the most likely explanation for their higher $^{87}Sr/^{86}Sr$ ratios than increased weathering of soil phyllosilicate minerals.

Based on the data presented in Bélanger et al. (2002a), the average uptake rate of Ca in the forest stand at HEW calculated over seventy-five years of growth using aboveground biomass and Ca concentrations in wood and foliage is about 2500 mol ha^{-1} yr^{-1}, with approximately two thirds of Ca returning annually to the forest floor as litterfall (~1700 mol ha^{-1} yr^{-1}). On the one hand, the bulk atmospheric Ca flux (30 to 80 mol ha^{-1} yr^{-1}) is less than 3% of that uptake flux (Bélanger et al., 2002a). On the other hand, the soil mineral weathering Ca, Mg and K fluxes were estimated using the SAFE model with a full set of measured input parameters including soil solution chemistry and soil moisture, texture and mineralogy (Bélanger et al., 2002b). The combined flux of Ca, Mg and K was estimated to be between 900 and 1150 mol ha^{-1} yr^{-1}. The Ca flux was 90% of the combined flux (N. Bélanger, unpublished data), which is approximately 800 to 1000 mol Ca ha^{-1} yr^{-1} or about 30% of the annual uptake rate of Ca. Despite the uncertainties in the soil mineral weathering estimates using this modeling approach, the fact that they are one order of magnitude larger than the atmospheric deposition flux supports the larger role of the soil mineral weathering flux as a source of Ca for the trees at the site.

The atmospheric and soil mineral weathering fluxes are nevertheless not large enough to satisfy the overall forest stand Ca needs. The forest floor exchangeable Ca concentration is about 0.40 mol kg^{-1} and the forest floor bulk density is about 300 kg m^{-3} and varies from 5 to 10 cm in thickness, which means a depth-corrected density of 15 to 30 kg m^{-3}. Through litter additions, a large forest floor Ca pool of 60 to 120 kmol ha^{-1} has built over time. This pool should therefore be regarded as the most significant accessible pool of Ca for the trees (Blum et al., 2008), built over time from litterfall (and throughfall) and composed of Ca originating from the atmosphere and soil minerals. At this stage in the development of the stand, the atmospheric and soil mineral weathering fluxes appear as complementary sources to litterfall, helping to replenish the forest floor exchangeable Ca pool on an annual basis. The litterfall Ca flux is 1.5 to 3% of that pool, whereas the soil mineral and atmospheric Ca fluxes are 0.8 to 1.5% and 0.02 to 0.1%, respectively.

Acknowledgement

This research was funded by the Fonds FCAR(now FQRNT), the Ministère des Ressources Naturelles du Québec (MRNQ), and the Natural Sciences and Engineering Research Council of Canada (NSERC). We thank Marie-Claude Turmel, Hélène Lalande, Pascale Legrand and Sylvie Manna for laboratory analyses and field assistance. Special thanks to Antonio Simonetti and Robert Creaser from the Radiogenic Isotope Facility in the Department of Earth & Atmospheric Sciences at the University of Alberta for performing the Sr isotopic analyses of our samples. Finally, we thank Marc Girard for preparing Figure 1.

References

Alban, D.H., 1982. Effects of nutrient accumulation by aspen, spruce, and pine on soil properties. Soil Sci. Soc. Am. J. 46, 853–861.

Ali, G., Roy, A.G., Turmel, M.C., Courchesne, F., 2010. Source-to-stream connectivity assessment through end-member mixing analysis. J. Hydrol. 392, 119–135.

Bailey, S.W., Hornbeck, J.W., Driscoll, C.T., Gaudette, H.E., 1996. Calcium inputs and transport in a base-poor forest ecosystem as interpreted by Sr isotopes. Water Resour. Res. 32, 707–719.

Barton J.M. Jr., Doig R., 1977. Sr-isotopic studies of the origin of the Morin Anorthosite Complex, Quebec, Canada. Contrib. Mineral. Petrol. 61, 219–230.

Beauregard, F., Côté, B., 2008. Test of soil extractants for their suitability in predicting Ca/Sr ratios in leaves and stems of sugar maple seedlings. Biogeochemistry 88, 195–203.

Bélanger, N., Côté, B., Courchesne, F., Fyles, J.W., Warfvinge, P., Hendershot, W.H., 2002a. Simulation of soil chemistry and nutrient availability in a forested ecosystem of southern Quebec. Part I. Reconstruction of the time-series files of nutrient cycling using the MAKEDEP model. Environ. Model. Soft. 17, 427–445.

Bélanger, N., Courchesne, F., Côté, B., Fyles, J.W., Warfvinge, P., Hendershot, W.H., 2002b. Simulation of soil chemistry and nutrient availability in a forested ecosystem of southern Quebec. Part II. Application of the SAFE model. Environ. Model. Soft. 17, 445–467.

Bélanger, N., Côté, B., Fyles, J.W., Courchesne, F., Hendershot, W. H., 2004. Forest regrowth as the controlling factor of soil nutrient availability 75 years after fire in a deciduous forest of Southern Quebec. Plant Soil 262, 363–372.

Bélanger, N., Holmden, C., 2010. Influence of landscape on the apportionment of Ca nutrition in a Boreal Shield forest of Saskatchewan (Canada) using $^{87}Sr/^{86}Sr$ as a tracer. Can. J. Soil Sci. 90, 267–288.

Bern, C.R., Townsend, A.R., Farmer, G.L., 2006. Unexpected dominance of parent-material strontium in a tropical forest on highly weathered soils. Ecology, 86, 626–632.

Biron, P.M., Roy, A.G., Courschesne, F., Hendershot, W.H., Côté, B., Fyles, J.W., 1999. The effects of antecedent moisture conditions on the relationship of hydrology to hydrochemistry in a small forested watershed. Hydrol. Process. 13, 1541–1555.

Blum, J.D., Klaue, A., Nezat, C.A., Driscoll, C.T., Johnson, C.E., Siccama, T.G., Eagar, C., Fahey, T.J., Likens, G.E., 2002. Mycorrhizal weathering of apatite as an important calcium source in base-poor forest ecosystems. Nature 417, 729–731.

Blum, J.D., Erel, Y., 1997. Rb-Sr isotope systematics of a granitic soil chronosequence: The importance of biotite weathering. Geochim. Cosmochim. Acta 61, 3193–3204.

Boulet, G., Jacques, G., 1992. Programme d'échantillonnage des précipitations du Québec: sommaire des données de la qualité des eaux de précipitations, 1989. Direction des Réseaux Atmosphériques, Ministère de l'Environnement du Québec, Rapport QEN/PA-45.

Bullen, T.D., Bailey, S.W., 2005. Identifying calcium sources at an acid deposition-impacted spruce forest: a strontium isotope, alkaline earth element multi-tracer approach. Biogeochemistry 74, 63–99.

Burns, R.M., Honkala, B.H., 1990. Silvics of North America: 2. Hardwoods. Agricultural Handbook 654, Volume 2, U.S. Department of Agriculture, Forest service, Washington.

Buzon, M.R., Simonetti, A., Creaser, R.A., 2007. Migration in the Nile Valley during the New Kingdom Period: A preliminary strontium isotope analysis. J. Archaeol. Sci. 34, 1391–1401.

Capo, R.C., Stewart, B.W., Chadwick, O.A., 1998. Strontium isotopes as tracers of ecosystem processes: theory and methods. Geoderma 82, 197–225.

Côté, B., Hendershot, W.H., Fyles, J.W., Roy, A.G., Bradley, R., Biron, P.M., Courchesne, F., 1998. The phenology of fine root growth in a maple-dominated ecosystem: relationships with some soil properties. Plant Soil 201, 59–69.

Côté, B., Bélanger, N., Courchesne, F., Fyles, J.W., Hendershot, W.H., 2003. A cyclical but asynchronous pattern of fine root and woody biomass production in a hardwood forest of southern Quebec and its relationships with annual variation of temperature and nutrient availability. Plant Soil 250, 49–57.

Courchesne, F., Côté, B., Fyles, J.W., Hendershot, W.H., Biron, P.M., Roy, A.G., Turmel, M.-C., 2005. Recent changes in soil chemistry in a forested ecosystem of southern Québec, Canada. Soil Sci. Soc. Am. J. 69, 1298–1313.

Creaser, R.A., Grutter, H.S., Carlson J., Crawford, B., 2004. Macrocrystal phlogopite Rb-Sr dates for the Ekati property kimberlites: Evidence for multiple intrusive episodes during Paleocene and Eocene time. Lithos 76, 399–414.

Dijkstra, F.A., Smits, M.M., 2002. Tree species effects on calcium cycling: The role of calcium uptake in deep soils. Ecosystems 5, 385–398.

Doig, R., 1991. U-Pb Zircon dates of Morin anorthosite suite rocks, Grenville Province, Quebec. J. Geology 99, 729–738.

Drouet, Th., Herbauts, J., Gruber, W., Demaiffe, D., 2005. Strontium isotope composition as a tracer of calcium sources in two forest ecosystems in Belgium. Geoderma 126, 203–223.

Drouet, T., Herbauts, J., Gruber, W., Demaiffe, D. 2007. Natural strontium isotope composition as a tracer of weathering patterns and of exchangeable calcium sources in acid leached soils developed on loess of central Belgium. Eur. J. Soil Sci. 58, 302–319.

Gaillardet J., Dupre B., Louvat P., Allegre C.J., 1999. Global silicate weathering and CO_2 consumption rates deduced from the chemistry of large rivers. Chem. Geol., 159, 3–30.

Hendershot, W.H., Courchesne, F., 1991. Comparison of soil solution chemistry in zero tension and ceramic-cup tension lysimeters. J. Soil Sci. 42, 577–583.

Holmden, C., Creaser, R.A., Muehlenbachs, K.M., 1997. Paleosalinities in ancient brackish water systems determined by $^{87}Sr/^{86}Sr$ ratios in carbonate fossils: a case study from the Western Canada Sedimentary Basin. Geochim. Cosmochim. Acta 61, 2105–2118.

Holmden, C., Bélanger, N., 2010. Ca isotope cycling in a forested ecosystem. Geochim. Cosmochim. Acta 74, 995–1015.

Hurlbut, C.S., Klein, C., 1985. Manual of mineralogy, 20th edition. John Wiley and Sons, New York.

Joslin, J.D., Kelly, J.M., Van Migroet, H., 1992. Soil chemistry and nutrition in North American spruce-fir stands. J. Env. Qual. 21, 12–30.

Kennedy, M.J., Chadwick, O.A., Vitousek, P.M., Derry, L.A., Hendricks, D.M., 1998. Changing sources of base cations during ecosystem development, Hawaiian Islands. Geology 26, 1015–1018.

Kennedy, M.J., Hedin, L.O., Derry, L.A., 2002. Decoupling of unpolluted temperate forest from rock nutrient sources revealed by natural $^{87}Sr/^{86}Sr$ and ^{84}Sr tracer addition. Proc. North Am. Acad. Sc. 99, 9639–9644.

Kittrick, J.A., Hope, E.W. 1963. A procedure for the particle-size separation of soils for X-ray diffraction analysis. Soil Science 96, 319–325.

Kobe, R.K., Pacala, S.W., Silander, J.A. Jr, Canham, C.D., 1995. Juvenile tree survivorship as a component of shade tolerance. Ecol. Appl. 5, 517–532.

Likens, G.E., Driscoll, C.T., Buso, D.C., 1996. Long-term effects of acid rain: response and recovery of a forest ecosystem. Science 272, 244–246.

McCourt, G.H., 1993. Acidification and buffering mechanisms in soil ecosystems. M. Sc. thesis, McGill University, Department of Renewable Resources.

Miller, E.K., Blum, J.D., Friedland, A.J., 1993. Determination of soil exchangeable-cation loss and weathering rates using Sr isotopes. Nature 362, 438–441.

Nakano, T., Yokoo, Y., Yamanaka, M., 2001. Strontium isotope constraint on the provenance of basic cations in soil water and stream water in the Kawakami volcanic watershed, central Japan. Hydrol. Proces. 15, 1859–1875.

Nezat, C.A., Blum, J.D., Yanai, R.D., Hamburg, S.P., 2007. A sequential extraction to determine the distribution of apatite in granitoid soil mineral pools with application to weathering at the Hubbard Brook Experimental Forest, NH, USA. Appl. Geochem. 22, 2406–2421.

Nezat, C.A., Blum, J.D., Yanai, R.D., Park, B.B., 2008. Mineral sources of calcium and phosphorus in soils of the northeastern United States. Soil Sci. Soc. Am. J. 72, 1786–1794.

O'Brien, C., Hendershot, W.H., 1993. Separating streamflow into groundwater, solum and upwelling flow and its implications for hydrochemical modelling. J. Hydrol. 146, 1–12.

Parker, G.G., 1983. Throughfall and stemflow in the forest nutrient cycle. Adv. Ecol. Res. 13, 57–133.

Peck, W.H., DeAngelis, M.T., Meredith, M.T., Morin, E., 2005. Polymetamorphism of marbles in the Morin terrane, Grenville Province, Quebec. Can. J. Earth Sci. 42, 1949–1965.

Perakis, S.S., Maguire, D.A., Bullen, T.D., Cromack, K., Waring, R.H., Boyle, J.R., 2006. Coupled nitrogen and calcium cycles in forests of the Oregon Coast Range. Ecosystems 9, 63–74.

Pett-Ridge, J.C., Derry, L.A., Kurtz, A.C. 2009a. Sr isotopes as a tracer of weathering processes and dust inputs in a tropical granitoid watershed, Luquillo Mountains, Puerto Rico. Geochim. Cosmochim. Acta. 73, 25–43.

Pett-Ridge, J.C., Derry, L.A., Barrows, J.K., 2009b. Ca/Sr and 87Sr/86Sr ratios as tracers of Ca and Sr cycling in the Rio Icacos watershed, Luquillo Mountains, Puerto Rico. Chem. Geology 267, 32–45.

Philpotts, A.R., 1966. Origin of the anorthosite-mangerite rocks in southern Quebec. J. Petrology 7, 1-64.

Poszwa, A., Ferry, B., Dambrine, E., Pollier, B., Wickman, T., Loubet, M., Bishop, K., 2004. Variations of bioavailable Sr concentration and $^{87}Sr/^{86}Sr$ ratio in boreal forest ecosystems. Role of biocycling, mineral weathering and depth of root uptake. Biogeochemistry 67, 1–20.

Poszwa, A., Ferry, B., Pollie, B., Grimaldi, C., Pierre, C.-D., Loubet, M., Dambrine, E., 2009. Variations of plant and soil $^{87}Sr/^{86}Sr$ along the slope of a tropical inselberg. Ann. For. Sci. 66, 1–13.

Sharp, M., Creaser, R.A., Skidmore, M., 2002. Strontium isotope composition of runoff from a glacierized carbonate terrain. Geochim. Cosmochim. Acta 66, 595–614.

Simonetti, A., Gariépy, C., Carignan, J., 2000. Pb and Sr isotopic compositions of snowpack from Québec, Canada: Inferences on the sources and deposition budgets of atmospheric heavy metals. Geochim. Cosmochim. Acta 64, 5–20.

Simonetti, A., Buzon, M.R., Creaser, R.A., 2008. In-situ elemental and Sr isotope investigation of human tooth enamel by laser ablation-(MC)-ICP-MS: Successes and pitfalls. Archaeometry 50, 371–385.

Soil Classification Working Group, 1998. The Canadian system of soil classification. Agriculture and Agri-Food Canada, Publication 1646 (Revised), 3rd edition, NRC Research Press, Ottawa, Ontario.

Stewart, B.W., Capo, R.C., Chadwick, O.A., 1998. Quantitative strontium isotope models for weathering, pedogenesis and biogeochemical cycling. Geoderma 82, 173–195.

Sverdrup, H., Warfvinge, P. 1992. Critical loads. *In* Modelling groundwater response to acidification. *Edited by* P. Sandén and P. Warfvinge. Swedish Meteorological and Hydrological Institute, Norrköping, Sweden. Rep. 5. pp. 171–186.

Thiffault, E., Paré, D., Bélanger, N., Munson, A.D., Marquis, F., 2006. Harvesting intensity in the boreal forest: impacts on soil nutrient availability and tree nutrition. Soil Sci. Soc. Am. J. 70, 691–701.

van Breemen, N, Finzi, A.C., Canham, C.D., 1997. Canopy tree – soil interactions within temperate forests: effects of soil elemental composition and texture on species distributions. Can. J. For. Res. 27, 1110–1117.

Veillette, J.J., 2004. Ice-Flow Chronology and Palimpsest, Long-Distance Dispersal of Indicator Clasts, North of the St. Lawrence River Valley, Quebec. Géogr. Phys. Quat. 58, 187-216.

Vitousek, P.M., Kennedy, M.J., Derry, L.A., Chadwick, O.A., 1999. Weathering versus atmospheric sources of strontium in ecosystems on young volcanic soils. Oecologia 121, 255–259.

Wilson, M.J., 2004. Weathering of the primary rock-forming minerals: processes, products and rates. Clay Minerals 39, 233–266.

Table 1. Bulk chemistry of the local anorthosite and of the soils in the three zones of the Hermine Experimental Watershed.

	Units	Anorthosite	Zone 1	Zone 2	Zone 3
SiO_2	%	53.5	65.3	61.3	65.9
TiO_2		0.34	0.85	0.78	0.97
Al_2O_3		23.4	14	15.3	14.1
Fe_2O_3*		3.33	5.32	4.91	5.55
MnO		0.051	0.071	0.065	0.074
MgO		2.36	1.45	1.35	1.53
CaO		11	3.13	2.64	3.31
Na_2O		4.23	2.63	2.5	2.64
K_2O		0.72	2.41	2.54	2.39
P_2O_5		0.019	0.15	0.14	0.16
BaO	$\mu g\ g^{-1}$	201	656	719	653
Rb		4.9	46.6	50.2	46.2
Sr		680	259	248	272

*Total iron present has been recalculated as Fe_2O_3. In cases where most of the iron was originally in the ferrous state (usually the case with unaltered rocks), a higher total is the result.

Table 2. Strontium, calcium, barium and $^{87}Sr/^{86}Sr$ in waters at the Hermine Experimental Watershed.

Sample	Zone no./Plot no.	Month/ (no. samples)	Year	$^{87}Sr/^{86}Sr$	Ba	Sr	Ca	Ca/Sr	Ba/Sr
					mg/L	mg/L	mg/L	mol/mol	mol/mol
Bulk deposition (tower)		Jan.-April (6×)	2004	0.71334	0.0610	0.0021	0.20	215	18.7
Bulk deposition (tower)		Aug.-Sept. (4×)	2004	0.71282	0.0439	0.0017	0.26	346	16.7
Bulk deposition (tower)		Sept.-Oct. (4×)	2004	0.71197	0.0392	0.0020	0.47	498	12.2
Bulk deposition (tower)		Oct.-Nov. (4×)	2004	0.71200	0.0267	0.0014	0.31	502	12.5
Bulk deposition (tower)		Dec. (2×)	2004	0.70974	0.0008	0.0005	0.14	664	1.04
Wet deposition (Ecotech sampler)		May 7 - 9	2009	0.70979	0.0005	0.0004	0.08	489	0.86
Wet deposition (Ecotech sampler)		June 12 - 14	2009	0.70948	0.0007	0.0005	0.07	338	0.99
Bulk deposition (tower)		May 25	2009	0.71015	0.0007	0.0009	0.29	732	0.52
Bulk deposition (tower)		May 26	2009	0.70952	0.0007	0.0008	0.24	675	0.56
Bulk deposition (tower)		June 3	2009	0.70924	0.0005	0.0005	0.14	592	0.62
Bulk deposition (tower)		June 25	2009	0.70902	0.0011	0.0015	0.53	779	0.46
Wet deposition (provincial sampler)		June 9	2009	0.71036	0.0016	0.0018	0.50	614	0.58
Wet deposition (provincial sampler)		June 16	2009	0.70898	0.0008	0.0008	0.31	849	0.68
Wet deposition (provincial sampler)		June 23	2009	0.70868	0.0013	0.0005	0.10	472	1.86
			Average	0.71036	0.0128	0.0011	0.261	555	4.88
			1s	0.00152	0.0208	0.0006	0.152	180	6.84
Throughfall	Z1/P2	May-Aug. (6×)	2004	0.71092	0.155	0.0096	1.35	307	10.3
Throughfall	Z1/P2	Sept.-Nov. (5×)	2004	0.70946	0.109	0.0079	1.29	356	8.80
Throughfall	Z3/P7	May-Aug. (6×)	2004	0.71149	0.114	0.0055	0.96	379	13.1
Throughfall	Z3/P7	Sept.-Oct. (3×)	2004	0.71049	0.062	0.0039	0.73	409	10.1
Throughfall	Z3/P9	May-Aug. (6×)	2004	0.71109	0.109	0.0053	0.86	356	13.1
Throughfall	Z3/P9	Sept.-Nov. (5×)	2004	0.70977	0.068	0.0059	1.49	548	7.29
Lysimeter FF horizon	Z1/P2	May-July (4×)	2004	0.70856	0.093	0.0310	3.01	212	1.91
Lysimeter FF horizon	Z1/P2	Jul.-Nov. (6×)	2004	0.70819	0.083	0.0329	3.87	257	1.62
Lysimeter FF horizon	Z3/P7	March-July (5×)	2004	0.70943	0.088	0.0216	1.99	201	2.60
Lysimeter FF horizon	Z3/P7	Aug.-Nov. (5×)	2004	0.70915	0.114	0.0192	2.62	298	3.79
Lysimeter FF horizon	Z3/P9	Feb.-Apr. (3×)	2004	0.70929	0.121	0.0207	1.41	148	3.72
Lysimeter FF horizon	Z3/P9	May-Nov. (3×)	2004	0.70913	0.144	0.0227	2.08	201	4.06
Lysimeter B horizon	Z1/P2	Feb.-May (5×)	2004	0.70865	0.030	0.0096	1.05	239	2.00
Lysimeter B horizon	Z1/P2	June-Nov. (5×)	2004	0.70816	0.037	0.0113	1.22	235	2.08
Lysimeter B horizon	Z3/P7	Feb.-May (5×)	2004	0.70828	0.027	0.0130	1.70	286	1.32
Lysimeter B horizon	Z3/P7	June-Nov. (5×)	2004	0.70854	0.029	0.0144	1.42	216	1.28
Lysimeter B horizon	Z3/P9	Feb.-May (4×)	2004	0.70898	0.029	0.0128	1.43	245	1.44
Lysimeter B horizon	Z3/P9	June-Nov. (4×)	2004	0.70830	0.040	0.0153	1.87	267	1.66
Stream low flow		May-June (17×)	2004	0.70753	0.011	0.0155	2.14	302	0.45
Stream low flow		June-July (17×)	2004	0.70744	0.012	0.0179	2.49	305	0.43
Stream low flow		July-Aug. (20×)	2004	0.70785	0.017	0.0143	1.90	292	0.78
Stream low flow		Aug.-Sept. (12×)	2004	0.70774	0.036	0.0175	2.44	305	1.30
Stream medium flow		Sept. (12×)	2004	0.70787	0.044	0.0158	2.11	292	1.77
Stream medium flow		Oct. (14×)	2004	0.70772	0.026	0.0168	2.29	297	0.98
Stream medium flow		Oct.-Nov. (16×)	2004	0.70745	0.010	0.0159	2.24	308	0.39
Stream medium flow		Nov.-Dec. (11×)	2004	0.70741	0.006	0.0136	1.92	309	0.30
Stream high flow		March-Apr. (8×)	2004	0.70799	0.030	0.0137	1.86	296	1.40
Stream high flow		Apr. (7×)	2004	0.70799	0.036	0.0131	1.76	294	1.78
Stream high flow		Apr.-May (9×)	2004	0.70793	0.035	0.0136	1.83	293	1.64
Stream high flow		May (15×)	2004	0.70772	0.026	0.0150	2.03	296	1.11

*2004 samples are all bulked. The months represent the sampling period whereas the number of individual samples in parentheses are those used to make up the bulk sample.

Table 3. Strontium, calcium, barium and $^{87}Sr/^{86}Sr$ in stemwood and foliage at the Hermine Experimental Watershed.

Sample	Plot no.	Month	Year	$^{87}Sr/^{86}Sr$	Ca/Sr	Ba/Sr
					mol/mol	mol/mol
Stemwood						
Dowstream-downslope (zone 1)						
Yellow birch	1	May	2006	0.7078	200	2.26
Sugar maple	2	May	2006	0.7077	177	1.06
Sugar maple	2	May	2006	0.7077	180	1.13
American beech	2	May	2006	0.7079	298	1.72
American beech	3	May	2006	0.7080	234	1.53
Red maple	3	May	2006	0.7079	180	1.06
			Average	0.7078	212	1.46
			1s	0.0001	47.6	0.48
Dowstream-upslope (zone 3)						
Sugar maple	7	May	2006	0.7082	242	0.94
Red maple	7	May	2006	0.7086	338	1.04
Sugar maple	8	May	2006	0.7084	192	1.17
Red maple	8	May	2006	0.7083	292	1.38
White birch	8	May	2006	0.7086	276	2.26
Yellow birch	9	May	2006	0.7083	275	2.13
Yellow birch	9	May	2006	0.7083	291	2.19
Large tooth aspen	9	May	2006	0.7082	218	1.49
Large tooth aspen	9	May	2006	0.7080	231	0.97
White birch	9	May	2006	0.7082	250	2.23
			Average	0.7083	261	1.58
			1s	0.0002	42.4	0.56
Foliage						
Dowstream-downslope (zone 1)						
Sugar maple	1	August	2004	0.7076	327	0.62
Sugar maple	1	August	2004	0.7076	329	0.79
Sugar maple	1	August	2004	0.7075	323	0.45
Sugar maple	2	August	2004	0.7077	320	0.91
Sugar maple	2	August	2004	0.7079	320	0.58
Sugar maple	2	August	2004	0.7076	327	0.62
Sugar maple	2	August	2004	0.7076	294	0.58
Sugar maple	3	August	2004	0.7079	329	0.73
Sugar maple	3	August	2004	0.7076	364	0.89
Sugar maple	3	August	2004	0.7076	316	0.51
Red maple	1	August	2004	0.7076	503	0.63
American beech	3	August	2004	0.7078	507	0.72
			Average	0.7077	355	0.67
			1s	0.0001	71.9	0.14
Upstream-downslope (zone 2)						
Sugar maple	4	August	2004	0.7089	384	0.78
Sugar maple	4	August	2004	0.7090	424	0.76
Sugar maple	4	August	2004	0.7087	358	0.74
Sugar maple	5	August	2004	0.7088	320	0.58
Sugar maple	5	August	2004	0.7084	338	1.03
Sugar maple	5	August	2004	0.7085	351	1.02
Sugar maple	5	August	2004	0.7086	346	0.96
Sugar maple	5	August	2004	0.7086	392	0.95
Sugar maple	6	August	2004	0.7082	341	0.85
Sugar maple	6	August	2004	0.7083	386	0.90
Sugar maple	6	August	2004	0.7082	347	0.85
Red maple	5	August	2004	0.7084	852	0.76
			Average	0.7085	403	0.85
			1s	0.0003	144	0.13
Dowstream-upslope (zone 3)						
Sugar maple	7	August	2004	0.7082	385	0.71
Sugar maple	7	August	2004	0.7081	397	0.56
Sugar maple	8	August	2004	0.7083	377	0.78
Sugar maple	9	August	2004	0.7079	350	0.68
American beech	7	August	2004	0.7084	705	1.96
Yellow birch	7	August	2004	0.7082	495	1.93
Yellow birch	8	August	2004	0.7084	452	2.22
Yellow birch	9	August	2004	0.7080	504	2.80
Yellow birch	9	August	2004	0.7081	501	2.63
Yellow birch	9	August	2004	0.7081	501	2.63
White birch	8	August	2004	0.7081	509	1.33
Large tooth aspen	7	August	2004	0.7082	329	0.48
Large tooth aspen	9	August	2004	0.7079	279	0.59
Red maple	9	August	2004	0.7082	631	1.15
			Average	0.7082	458	1.46
			1s	0.0001	117	0.87

Table 4. Source apportionment calculations at the Hermine Experimental Watershed using the two scenarios of sources.

		$^{87}Sr/^{86}Sr$	molar Sr/Ca	molar Ca/Sr	Apportionment	
Mixing Scenario 1 — averaged atmospheric deposition vs. soil calcite and apatite						
Mixing end-members						
Atmospheric deposition		0.7104	1.70	588		
Soil calcite & apatite weathering		0.7070	0.62	1612		
Vegetation :					% atm.	% soil
Zone 2	upstream-downslope	0.7085			22	78
Zone 3	downstream-upslope	0.7081			15	85
Zone 1	downstream-downslope	0.7077			9	91
				average	15	85
Mixing Scenario 2 — soil mineral weathering between silicates & calcite/apatite						
Mixing end-members						
Soil silicate weathering		0.7111	1.37	730		
Soil calcite & apatite weathering		0.7070	0.62	1612		
Vegetation :					% silicates	% calcite/apatite
Zone 2	upstream-downslope	0.7085			21	79
Zone 3	downstream-upslope	0.7081			14	86
Zone 1	downstream-downslope	0.7077			9	91
				average	14	86

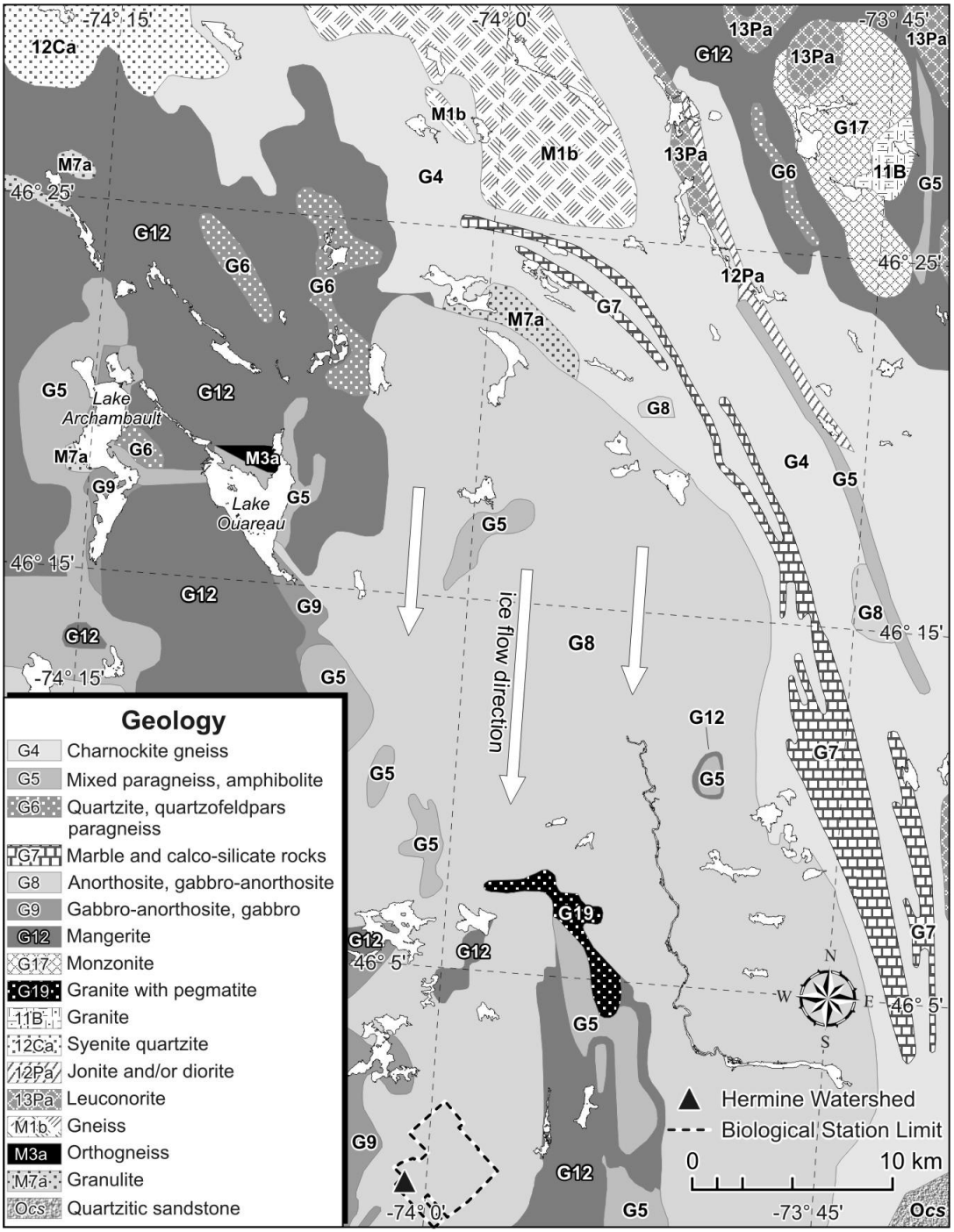

Figure 1. Location and geology of the Hermine Experimental Watershed and surroundings.

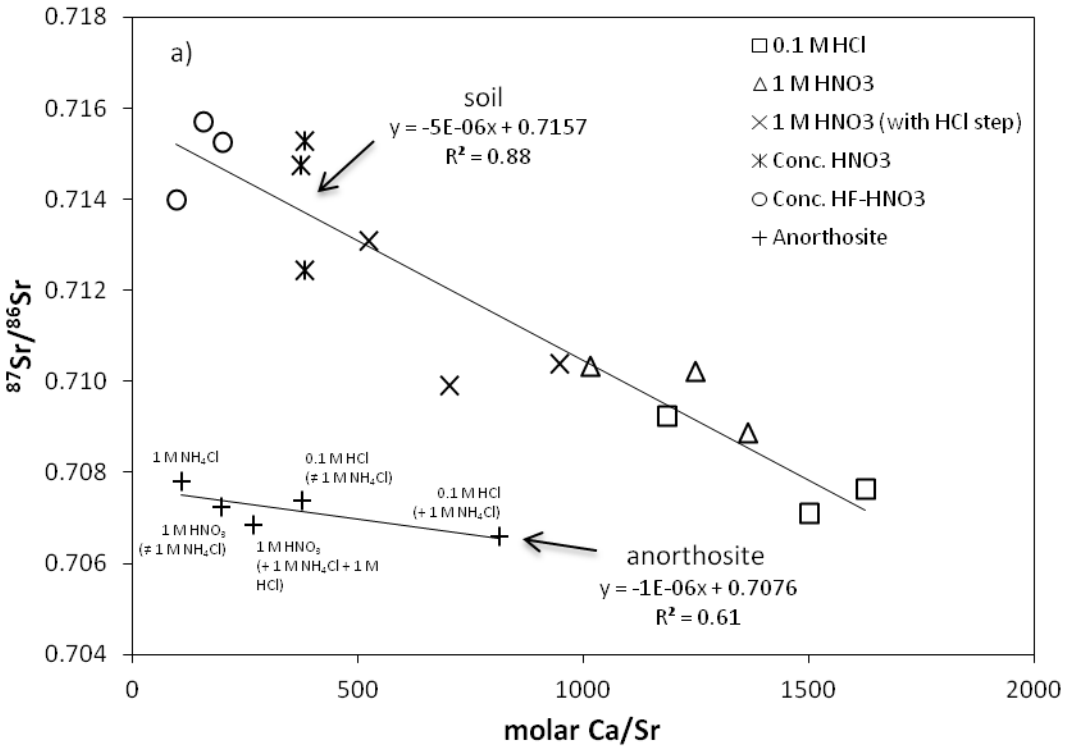

Figure 2. Relationships between $^{87}Sr/^{86}Sr$ and molar Ca/Sr ratios for acid leachates of soils and anorthosite. The line joining the + symbols is for leachates of anorthosite which are labelled to indicate the specific leach or sequential leaches.

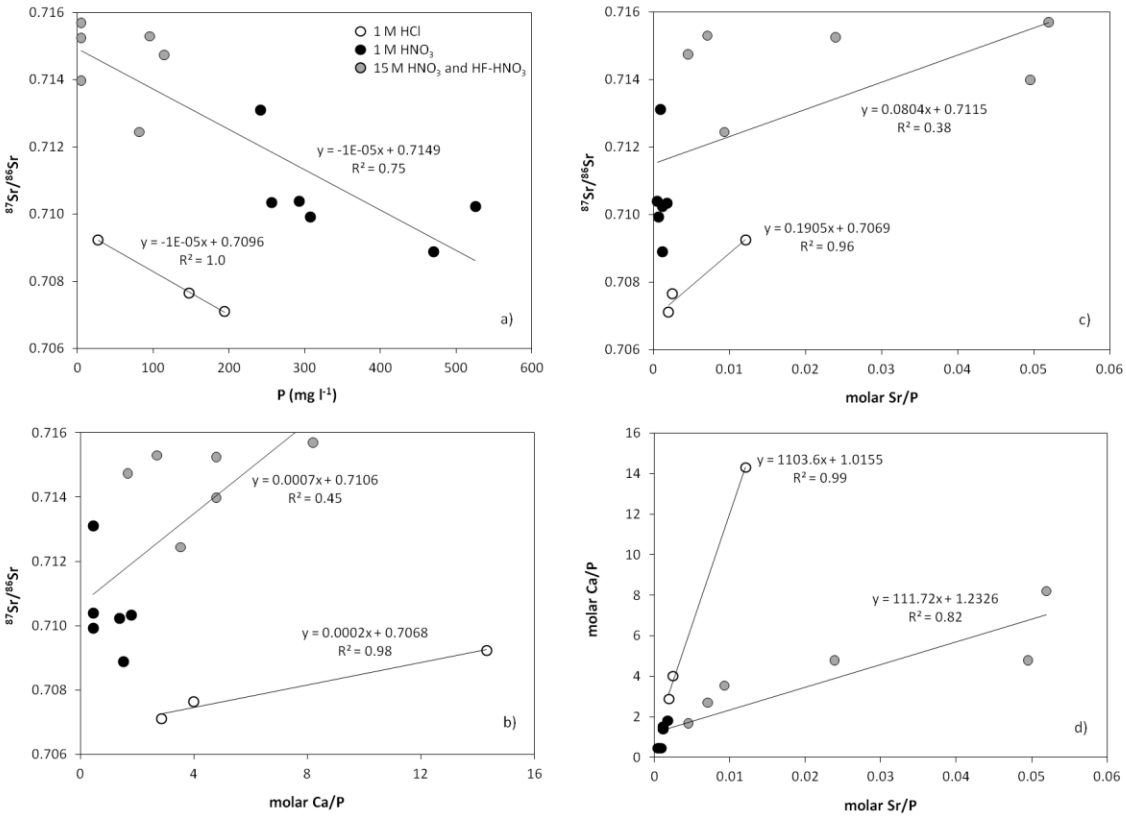

Figure 3. Relationships between $^{87}Sr/^{86}Sr$ ratios and P concentrations (a), molar Ca/P (b) and molar Sr/P (c) ratios; and between molar Ca/P vs. molar Sr/P ratios (d) in soil 0.1 M HCl and HNO_3 (1 M, concentrated, and HF mixture) leachates.

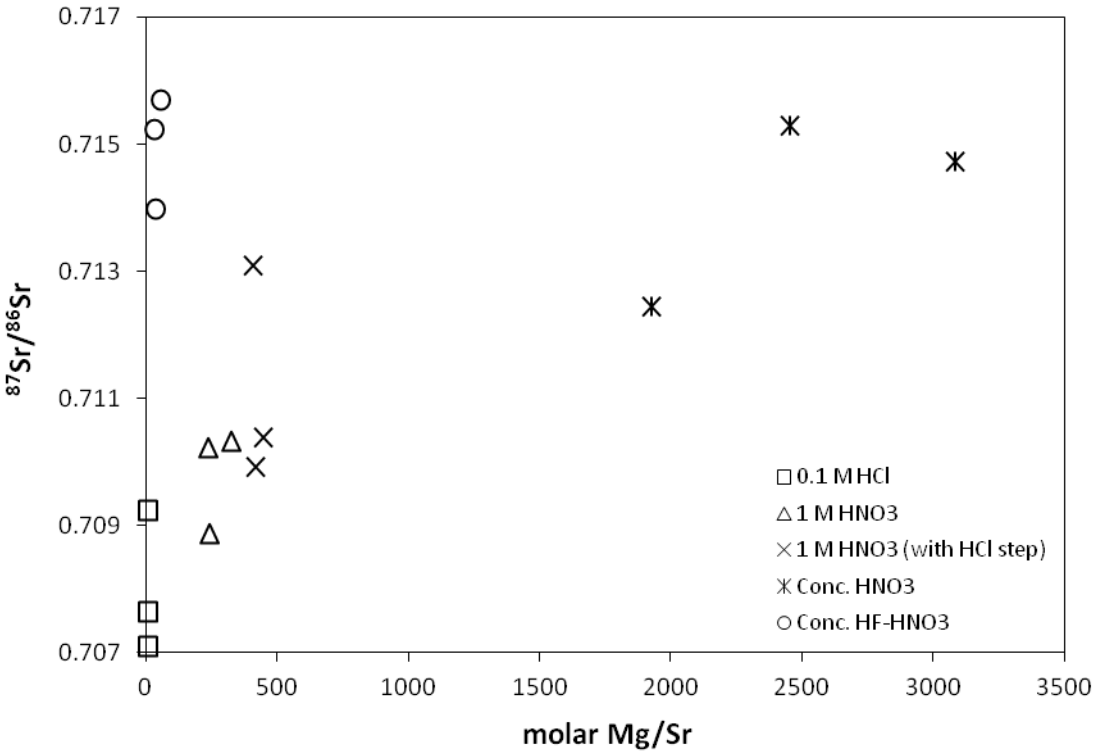

Figure 4. Relationships between $^{87}Sr/^{86}Sr$ and molar Mg/Sr ratios in acid leachates of soils.

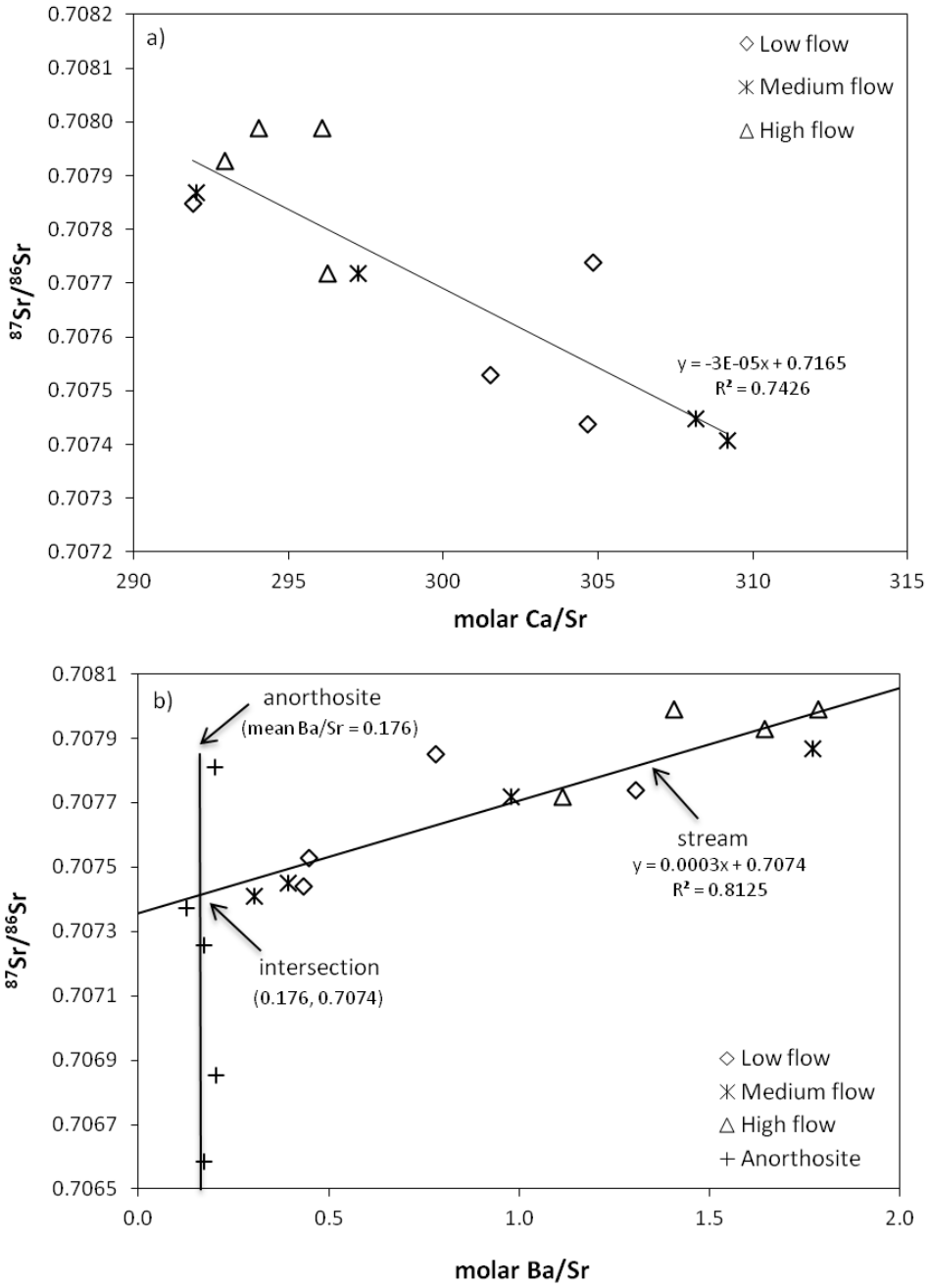

Figure 5. Relationships between $^{87}Sr/^{86}Sr$ ratios of stream water samples collected at low, medium and high flows and molar Ca/Sr (a) and molar Ba/Sr (b) ratios. In Figure 5b, the line joining the + symbols is for leachates of anorthosite.

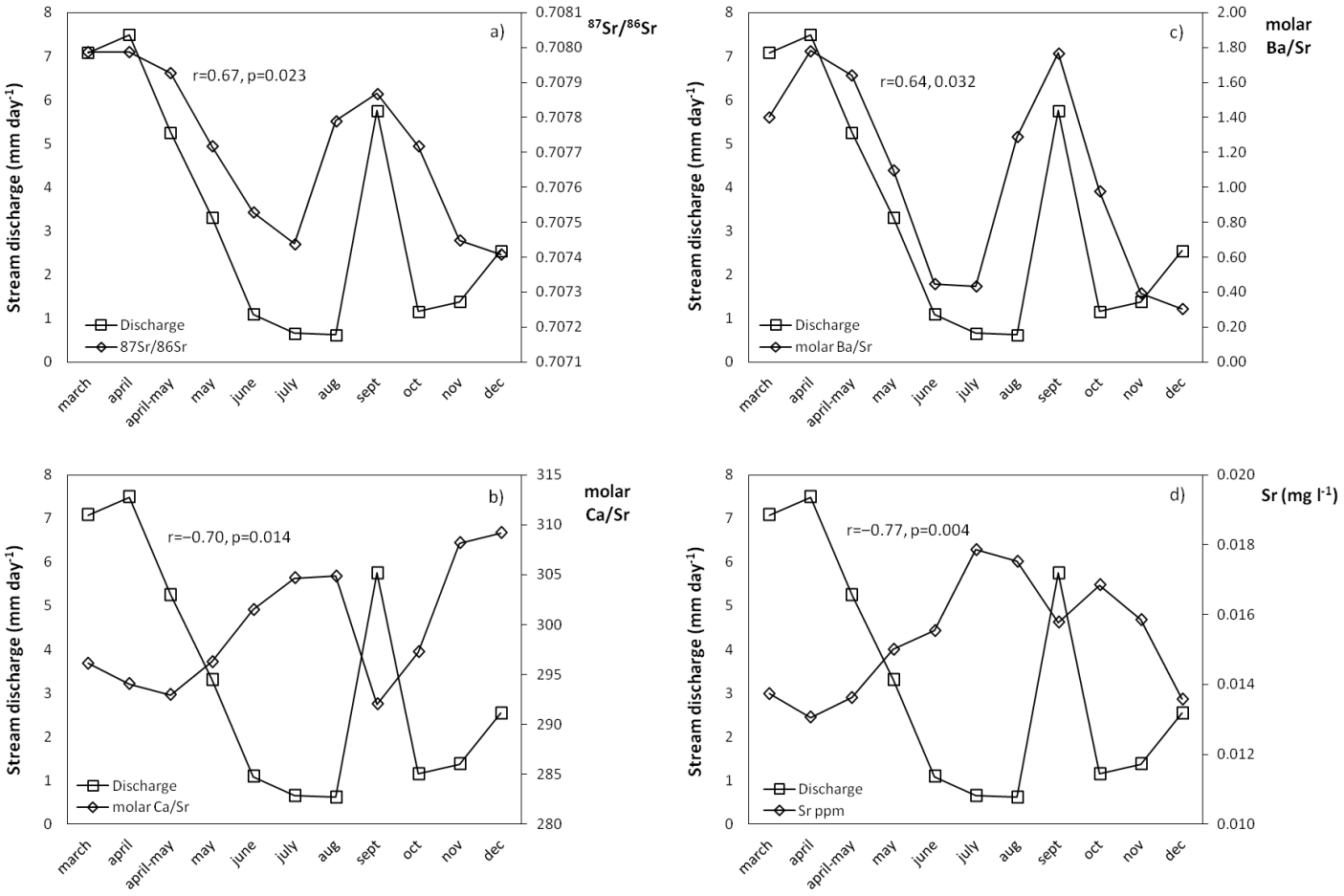

Figure 6. Relationship between stream discharge and stream water $^{87}Sr/^{86}Sr$ (a), molar Ca/Sr (b) and molar Ba/Sr (c) ratios and Sr concentrations during the 2004 hydrological year at the Hermine Experimental Watershed. Coefficient of correlations (r) and the levels of significance (p) between stream discharge and stream water $^{87}Sr/^{86}Sr$, molar Ca/Sr, molar Ba/Sr and Sr are given inside each panel.

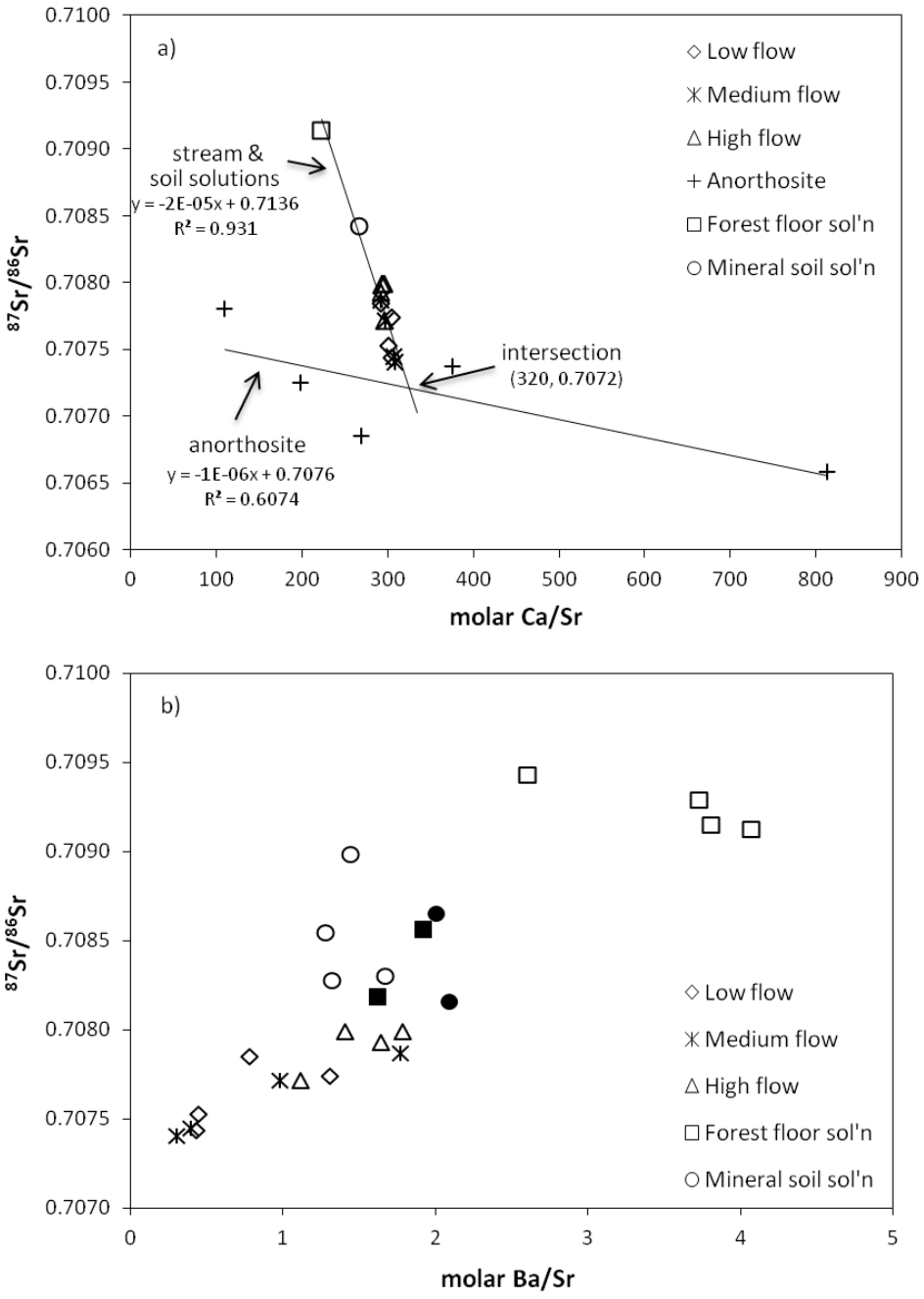

Figure 7. Relationships between $^{87}Sr/^{86}Sr$ ratios and molar Ca/Sr (a) and molar Ba/Sr (b) ratios for stream water and soil solution samples. In Figure 7a, the stream and soil solutions line is drawn using soil solution medians, whereas the line joining the + symbols is for leachates of anorthosite. In Figure 7b, the full squares and circles represent solution data from zone 1 (downstream-downslope).

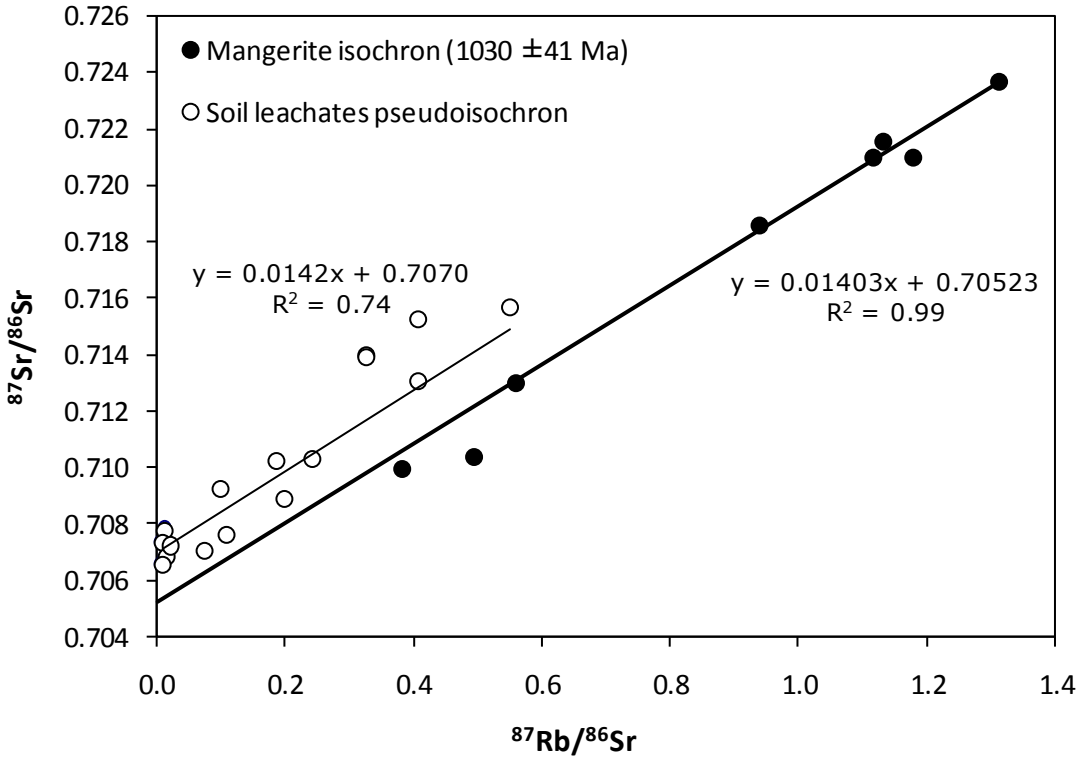

Figure 8. Relationships between the $^{87}Sr/^{86}Sr$ and $^{87}Rb/^{86}Sr$ ratios of soil and anorthosite acid leachates compared to the mangerite isochron in close proximity of the Hermine Experimental Watershed.